https://doi.org/10.5194/egusphere-2025-6552
Preprint. Discussion started: 23 January 2026

Aerosol Scavenging in DC3 and SEAC^{4}RS Deep Convective Storms

Mary C. Barth[1], Pedro Campuzano-Jost[2], Gustavo Cuchiara[3], Ajay Parottil[1,4], Jose L. Jimenez[2], Miguel Ricardo A. Hilario[5,6], Genevieve Rose Lorenzo[5,7], Armin Sorooshian[5,8]

[1]NSF National Center for Atmospheric Research, Boulder, Colorado 80307-3000 USA
[2]CIRES and Department of Chemistry, University of Colorado, Boulder, Colorado 80309-0216 USA
[3]Air Pollution Control Division, Colorado Department of Public Health and Environment, Denver, Colorado 80246-1523 USA
[4]Now at: Meteorology Department, Abu Dhabi Polytechnic, Abu Dhabi, UAE
[5]Department of Hydrology and Atmospheric Sciences, University of Arizona, Tucson, Arizona 85721 USA
[6]Now at: Space Science and Engineering Center, University of Wisconsin-Madison, Madison, WI 53706 USA
[7]Now at: Department of Atmospheric Sciences, Rosenstiel School, University of Miami, Miami, Florida, 33149 USA
[8]Department of Chemical and Environmental Engineering, University of Arizona, Tucson, Arizona 85721 USA

Correspondence to: Mary C. Barth (barthm@ucar.edu)

Abstract. Convective storms frequently occur over the central US during the late spring and summer impacting upper tropospheric composition, which in turn affects the radiative forcing of the climate system. Two important processes in deep convection are vertical transport and removal of trace gases and aerosols by microphysical scavenging. We calculate scavenging efficiencies of speciated aerosol mass concentrations based primarily on aircraft observations from the Deep Convective Clouds and Chemistry (DC3) and the Studies of Emissions, Atmospheric Composition, Clouds and Climate Coupling by Regional Surveys (SEAC^{4}RS) field experiments combined with process-scale modeling. Sulfate and ammonium scavenging efficiencies are generally greater than 75% for all storms analyzed. Particulate nitrate scavenging efficiencies are moderate (~40%). In some cases, the particulate nitrate concentrations are larger in the storm outflow region compared to the inflow region. Further analysis shows the role of entrainment of mid-tropospheric particulate nitrate layers and lightning production of nitrogen oxides in affecting the particulate nitrate outflow concentrations. Organic aerosol scavenging efficiencies are greater than 75% in severe storms, comparable to sulfate and ammonium, but ~50% for weak and moderate storms. Production of organic acids in cloud water is shown to contribute to organic aerosol mass in the outflow regions for the mid-day storms sampled, which may explain why those storms have lower apparent scavenging efficiencies. These results, which highlight the complex interactions between dynamics, physics, and chemistry in thunderstorms, can be used by chemistry transport models as a way to evaluate convective storm processing of aerosols.

1 Introduction

It is well recognized that atmospheric aerosols play an important role in climate, weather, and air quality (e.g., IPCC 2021; Seinfeld and Pandis, 2016). Thus, it is important to understand aerosol concentrations and properties, which are determined by the sources and sinks of the different types and sizes of aerosols. Sources of primary aerosols, such as dust, sea salt, primary organic aerosol (POA), and black carbon (BC), are from emissions, while secondary aerosols, such as accumulation

https://doi.org/10.5194/egusphere-2025-6552
Preprint. Discussion started: 23 January 2026

mode sulfate (SO_4^{2-}), particulate nitrate (pNO_3), and organics (SOA), are produced through chemical and physical processes. Although these sources and transport of aerosols have uncertainties associated with them, reducing the uncertainty associated with the wet and dry deposition of aerosols is equally important as these processes control the lifetime of aerosols in the atmosphere (Textor et al., 2006) and by extension aerosol-related effects on radiative forcing and clouds. Global chemistry transport models (CTMs) and chemistry-climate models have shown that aerosol wet deposition is the dominant atmospheric aerosol sink (e.g., Seinfeld and Pandis, 2016). Wet deposition occurs in synoptic-scale weather systems, stratiform clouds, and convective storms. To represent this important sink, regional-scale and global-scale CTMs must reasonably simulate vertical transport and scavenging of aerosols. Of the three types of precipitation systems mentioned, determining vertical transport and scavenging in convective storms is the most challenging for CTMs as they parameterize convective processes on the sub-grid scale. Here, we aim to advance our knowledge on convective cloud processing of aerosols via analysis of measurements taken in the inflow and upper troposphere outflow regions of convective storms.

Deep convective clouds provide an important and efficient mechanism for vertical transport and redistribution of tropospheric particles and trace gases (Dickerson et al., 1987; Yang et al., 2015). The convectively driven vertical transport of aerosols and trace gases from the atmospheric boundary layer (BL) to the upper troposphere can occur on timescales of a few minutes to an hour (Skamarock et al., 2000; Bela et al., 2018) leading to a rapid change in the abundance of aerosols and trace gases transported to the upper troposphere. As the air is lofted in convective updrafts, aerosols and soluble trace gases are incorporated into the cloud particles and removed from the atmosphere via precipitation (Flossmann et al., 1985). The representation of aerosol wet scavenging in CTMs includes nucleation, impaction, and Brownian diffusion scavenging. Nucleation scavenging, also known as cloud-drop activation and in-cloud scavenging, depends on the number of cloud condensation nuclei and supersaturation of the air (Jensen et al., 1984). The conversion of cloud water to precipitating hydrometeors (rain, snow, and graupel) moves the aerosols from the cloud drops to falling precipitation resulting in wet deposition (Seinfeld and Pandis, 2016). Many global and regional-scale CTMs represent this removal mechanism in two steps, first representing the cloud drop activation and tracking aerosols in cloud water, and second computing the conversion rate of aerosols in cloud water to precipitation (e.g., Abdul-Razzak and Ghan, 2000). In cases like convection, cloud drop activation on aerosols entrained into the storm above cloud base occurs. Impaction scavenging is the collection of aerosols by falling precipitation and is represented by either the continuous collection equation or by a scavenging coefficient (Seinfeld and Pandis, 2016; Croft et al., 2009). Impaction scavenging is sometimes termed below-cloud scavenging in the scientific literature. Brownian diffusion also occurs between cloud particles and aerosols but is often small compared to nucleation and impaction scavenging (Flossmann et al., 1985). Aerosol wet scavenging schemes must also represent the evaporation of precipitation and therefore the transfer of aerosol components within cloud hydrometeors back to particles in the gaseous atmosphere (Seinfeld and Pandis, 2016; Mitra et al., 1992).

Aerosol wet scavenging is sensitive to the approaches used to represent this process and the grid resolution used in models. Gong et al. (2011) showed that particulate matter (PM) concentrations are strongly affected by the choice of aerosol activation schemes and moderately affected by the choice of scavenging coefficients for below-cloud scavenging of aerosols.

https://doi.org/10.5194/egusphere-2025-6552
Preprint. Discussion started: 23 January 2026

On the other hand, Jones et al. (2022) found that the choice of below-cloud scavenging schemes caused substantial changes in accumulation-mode dust lifetime (from 5.4 to 44 days). Schill et al. (2020) suggested that hydrophobic aerosol can be removed within a cloud via impaction scavenging, which improves model-measurement agreement of aerosol concentrations. Yu et al. (2019) also found improved model-measurement agreement when cloud drop activation on aerosols entrained into convection above cloud base was included in their CTM aerosol wet scavenging scheme. The uncertainties associated with aerosol scavenging also depend on how accurately cloud and convective physical and dynamical processes are represented in models, indicating a need for additional analysis of the role of this important sink in global and regional-scale models.

Aqueous-phase chemistry in cloud and rain drops can also increase aerosol mass concentrations (Hegg and Hobbs, 1981; 1982; Ervens et al., 2011). Conversion of aqueous-phase sulfur dioxide (SO_2) forms SO_4^{2-}, enhancing its mass concentration (Seinfeld and Pandis, 2016). As SO_4^{2-} production affects the drop acidity, NH_4^+ and pNO_3 concentrations in cloud water can change in response to the acidity change (Zheng et al., 2023). Further, pNO_3 and NH_4^+ concentrations within the cloud drops can increase from dissolution and subsequent dissociation of nitric acid (HNO_3) or organic nitrate gases and ammonia (NH_3). Formation in cloud water of SOA from aqueous oxidation of aldehydes and carboxylic acids and from aqueous epoxide chemistry is less well characterized because of the non-linear organic aqueous chemistry (e.g., McNeill, 2015; Tsui et al., 2019; Ervens et al., 2011; Blando and Turpin, 2000).

Previous studies have estimated aerosol wet scavenging efficiencies in various types of clouds. Since nucleation (or in-cloud) scavenging is often the dominant scavenging process (Ohata et al., 2016), comparisons of aerosol concentrations measured in the interstitial cloud air to those measured before a cloud or fog event or in the inflow region can be used to estimate scavenging (e.g., Noone et al., 1992). Similarly, comparisons of cloud water residual with interstitial aerosol concentrations can be used. Analyses of aerosol concentrations in the inflow and outflow regions of clouds have also estimated aerosol scavenging efficiencies (Hegg et al., 1984; Yang et al., 2015; Hilario et al., 2025). The scavenging efficiencies for aerosol SO_4^{2-}, NH_4^+, and pNO_3 generally ranged from 55 to 85%. Organic aerosol scavenging efficiencies have been estimated only recently (Yang et al., 2015; Hilario et al., 2025). Yang et al. (2015) found 80-84% scavenging for organic aerosols by a severe thunderstorm in Oklahoma, while Hilario et al. (2025) found 53-60% scavenging in shallow to moderate marine tropical convection near the Philippines. These previous studies each focused on a limited number of one to three case studies. Extending the analysis to several more convective storms as performed in this study should provide a more robust quantification of aerosol scavenging.

In this paper we quantify vertical transport and scavenging of aerosols through analysis of ten deep convective storms sampled over the central United States. The analysis uses a variety of measurements primarily obtained aboard the NASA DC-8 aircraft but also includes ground-based radar data and radiosonde data. These data are detailed in section 2. We next describe the analysis method, which employs an entrainment model (section 3). The cases investigated, described in section 4, span a range of convective types from severe convection to moderate and airmass storms. Before presenting estimates of scavenging efficiencies, we discuss the vertical profiles in clear air for the cases studied (section 5), as they are a key

https://doi.org/10.5194/egusphere-2025-6552
Preprint. Discussion started: 23 January 2026

component for the scavenging efficiency calculation. In the Results section, we show the scavenging efficiencies derived for each case for SO_4^{2-}, NH_4^+, pNO_3, and organic aerosol (OA). We discuss reasons for the lower pNO_3 scavenging efficiencies, including the role of particulate organic nitrates, a mid-troposphere pNO_3 layer that is not as pronounced for SO_4^{2-} or NH_4^+, and lightning-generated nitrogen oxides (NO_x = NO + NO_2) forming HNO_3 and its subsequent partitioning onto aerosols in the upper troposphere convective outflow region. We also explore whether aqueous phase chemistry affects the OA scavenging efficiencies in the Southeast United States.

2 Field measurements

Measurements are analyzed from the NSF/NASA Deep Convective Clouds and Chemistry (DC3; Barth et al., 2015) and the NASA Studies of Emissions and Atmospheric Composition, Clouds and Climate Coupling by Regional Surveys (SEAC^{4}RS; Toon et al., 2016) field experiments. The DC3 field campaign investigated the impact of deep, mid-latitude continental convective clouds, including their dynamical, physical, and lightning processes, on upper tropospheric composition and chemistry (Barth et al., 2015). The DC3 field campaign sampled storms in northeast Colorado and southwest Nebraska, central Oklahoma, and northern Alabama as well as a mesoscale convective system (MCS) occurring in the Missouri-Arkansas-Mississippi area. The campaign utilized two aircraft platforms (NASA DC-8 and NSF/NCAR GV) to sample inflow, outflow, and clear sky composition as well as extensive ground-based observations to characterize the morphology, kinematics, and lightning activity of the storms. For this analysis, composition measurements from only the NASA DC-8 are analyzed as this aircraft hosted several instruments measuring the concentrations and properties of aerosols.

The SEAC^{4}RS campaign (Toon et al., 2016) included the goal of determining how pollutant emissions are redistributed via deep convection throughout the troposphere to understand how vertical transport modifies upper troposphere chemistry and composition. To achieve this goal, the NASA DC-8 sampled the inflow region and near-cloud-top region of convective storms occurring over the southern United States. The NASA DC-8 instruments used in this analysis are the same for both the SEAC^{4}RS and DC3 field campaigns.

2.1 Aircraft measurements

The NASA DC-8 aircraft measurements used in the aerosol scavenging analysis (Table S1, which also includes acronym definitions) include passive trace gases, such as carbon monoxide (CO; DACOM instrument, Sachse et al., 1987), carbon dioxide (CO_2; AVOCET instrument, Vay et al., 2011), n-, i-butane and n-, i-pentane, and other alkanes and alkenes (PTR-MS and WAS instruments, de Gouw and Warneke, 2007; Simpson et al., 2011), to determine both the connectivity between the BL and outflow air masses (using i- to n- ratios of butane and pentane) and the entrainment rate for the storm (Fried et al., 2016; Barth et al., 2016, Cuchiara et al., 2020). The wind components, temperature, pressure, and GPS altitude (MMS instrument, Chan et al., 1998) are used to provide environmental information for the analysis. Liquid or ice water content (FCDP and 2D-S instruments, Lawson et al., 2011) is used to determine when the DC-8 was in or out of cloud. Nitric acid

https://doi.org/10.5194/egusphere-2025-6552
Preprint. Discussion started: 23 January 2026

(HNO_3; CIT-CIMS instrument) is used for examining total inorganic nitrate scavenging. While SO_2 was also examined, its measured values in the outflow or upper troposphere clear sky were reported as missing values for the cases studied, preventing any calculations of total sulfur scavenging. More information on the use of these data is given in Barth et al. (2016) and Cuchiara et al. (2020).

In describing each storm case, several trace gases and aerosols were used to characterize the BL chemical environment. Isoprene and toluene (PTR-MS and WAS instruments) characterized the influence of biogenic and anthropogenic sources on the BL composition. The dry aerosol extinction (from the Langley Aerosol Research Group Experiment TSI 3563 integrating nephelometer, Wagner et al., 2015) for accumulation and coarse aerosols characterized the aerosol abundance (Barth et al., 2015) in the BL, while the OA fraction of particulate matter at <1 μm in size (PM_1) gave information on the composition of the aerosols. PM_1 is calculated as the sum of the aerosol mass spectrometer (AMS, DeCarlo et al., 2006; Guo et al., 2021) aerosol concentrations plus the HD-SP2 BC concentration (Schwarz et al., 2013). Other trace gases were used to remove influences from the stratosphere or biomass burning. The CO to ozone (O_3; CSD CL instrument, Ryerson et al., 2000; Pollack et al., 2011) ratios were used to filter out stratospheric influence. The influence of biomass burning air masses was removed (or included) based on concentrations of hydrogen cyanide (HCN; CIT-CIMS, Crounse et al., 2006) and acetonitrile (CH_3CN; PTR-MS). Aerosol number concentrations (SMPS instrument, Wang and Flagan, 1993), hydroxyl radical (OH; ATHOS instrument, Faloona et al., 2004), and peroxynitrates (MPN, ANs, PNs; TD-LIF instrument, Nault et al., 2015) were also examined for a few specific storm cases.

Aerosol mass concentrations of SO_4^{2-}, NH_4^+, pNO_3, and OA reported by the University of Colorado aircraft AMS (Canagaratna et al., 2007, DeCarlo et al., 2006) are analyzed in this work to derive scavenging efficiencies. The AMS chloride measurements are not discussed here because the chloride concentrations were negligible compared to the other AMS constituents measured and often at or below the detection limit. AMS 1 Hz detection limits during DC3 were generally in line with the ones reported for the same instrument in Guo et al. (2021) despite significant differences in the data acquisition setup, while for SEAC^{4}RS they were about two times higher, mostly due to the much more polluted conditions during that campaign. These detection limits were rigorously propagated for each storm sampling and data were flagged when average concentrations were below these detection limits, resulting in 100% scavenging efficiencies for those cases. This treatment had almost no impact on the DC3 cases discussed here, but limited the analysis of some SEAC^{4}RS storm samplings since the outflow intercept time periods were generally short (< 1 minute). Examination of the DC3 data showed that the AMS was insensitive to most artifacts associated with ice particle shattering when there was sufficient signal-to-noise (Yang et al., 2015). While the AMS samples PM_1 (see Guo et al., 2021 for a detailed description of PM_1 for these campaigns), the scavenging efficiencies determined here should be representative for all accumulation mode aerosols as the convective clouds have high supersaturations that should activate hygroscopic aerosols at sizes < 1 μm.

The AMS-reported pNO_3 includes both organic ($pRONO_2$) and inorganic (NO_3^-) nitrates (Day et al., 2022; Farmer et al., 2010). In this paper, we report separate efficiencies for both nitrate forms for cases where $pRONO_2$ or NO_3^- in both inflow and outflow were above the detection limit. While AMS-reported SO_4^{2-} can suffer from similar organic interferences

https://doi.org/10.5194/egusphere-2025-6552
Preprint. Discussion started: 23 January 2026

(Schueneman et al., 2021; Chen et al., 2019) that are harder to quantify, SO_4^{2-} scavenging efficiencies reported here should be considered for inorganic SO_4^{2-} only based on the agreement of the AMS with the SAGA MC-IC instrument (Dibb et al., 2003). The AMS data have been reprocessed for this work to incorporate processing refinements used in the analysis of more recent aircraft campaigns. This includes some features critical for this work, such as additional zero corrections and a refined pRONO2 apportionment.

2.2 Thermodynamic calculations with E-AIM

Significant aerosol acidity gradients typically exist between the BL, the free troposphere and convective outflow (Nault et al., 2021). This can impact the partitioning of NH_4^+ and NO_3^- between the gas and the aerosol phase (Guo et al., 2016; Pye et al., 2020) and hence cause uncertainties in convective transport efficiencies if one assumes a non-volatile aerosol (Yang et al., 2015). To quantify these possible biases, aerosol pH and nitrate partitioning factors are calculated using the E-AIM Model IV (Clegg et al., 1998; Friese and Ebel 2010) for the AMS aerosol data (using only apportioned NO_3^-) and gas-phase HNO_3 from the CIT-CIMS instrument, respectively, using the AMATI (Ambient Aerosol Thermodynamic calculator in Igor) package (Campuzano-Jost et al., 2021). Since no in-situ NH_3 data are available for either DC3 or SEAC^{4}RS, the same iterative approach as in Nault et al. (2021) was used to estimate NH_3 from the other inputs. This approach works well in acidic environments where HNO_3 partitioning is mostly controlling the pH (Pye et al., 2020; Li et al., 2024), which applies to most of the data reported here. Only the inorganic nitrate aerosol fractions $NO_3^-/(NO_3^- + HNO_3)$ in DC3 convective outflow regions are discussed in the results, as SO_4^{2-} and NH_4^+ are not volatile (Seinfeld and Pandis, 2016).

2.3 Ground-based measurements

For both DC3 and SEAC^{4}RS, the National Weather Service (NWS) Next Generation Weather Radar (NEXRAD) reflectivity is used in the analysis. The S-band data from multiple radars are composited into a 3-d product following the gridded NEXRAD algorithm (GridRad v3.1) described by Homeyer and Bowman (2017). Measurements of radar reflectivity are used to identify time periods when the aircraft was in the inflow and outflow regions of the storm. The NEXRAD data also provide storm characteristics, such as the maximum radar reflectivity in a column and storm height of the 20 dBZ level.

Radiosondes are analyzed to obtain information on the thermodynamic environment of the storm. During DC3, radiosondes were launched near the storms from mobile facilities, including the NCAR Mobile Integrated Sounding System for Colorado storms and the NOAA/NSSL mobile sounding system. One DC3 case also utilized the NWS operational radiosonde. For SEAC^{4}RS, the NWS operational radiosondes are used as well as analysis of DC-8 aircraft vertical profiles in clear air near the storms.

https://doi.org/10.5194/egusphere-2025-6552
Preprint. Discussion started: 23 January 2026

3 Determination of scavenging efficiency

The observational analysis for determining scavenging efficiency is a multistep process using an entrainment model that simply represents the mixing of an air parcel with the environment as it is lofted from cloud base to cloud top. This methodology extends the work of Cohan et al. (1999), Borbon et al. (2012), and Yang et al. (2015) from a two-, three-, and four-layer entrainment model approach, respectively, to a 7–10-layer (depending on the height of the storm) entrainment model that uses background air vertical profiles with improved vertical resolution. By having 1-km altitude bins, changes in the vertical distributions of the passive trace gas and aerosol species are better represented.

By sampling the composition of the air in the storm inflow, background free troposphere, and storm outflow regions (Fig. 1), entrainment rate can be estimated using passive trace gases that are insoluble and whose chemical lifetime is much longer than the transport time from cloud base to outflow sampling region. Mathematically, the entrainment rate $\boldsymbol{\alpha}$ (fraction km^{-1}) of background free troposphere air can be determined from

$$C_{(k)} = (1 - \boldsymbol{\alpha})C_{(k-1)} + \boldsymbol{\alpha}C_{FT(k)}, k = 1, \dots, N \quad (1)$$

where C is the mixing ratio at altitude bin k of the passive trace gas being lifted from cloud base (k=1) to cloud top (k=N), and C_{FT} is the passive trace gas mixing ratio in the free troposphere and varies with altitude. The values of k at the cloud base and top depend on the storm sampled. Cloud bases are 1.7-2.0 km MSL for Colorado storms, 1.0-1.3 km MSL for Oklahoma storms, and < 1.0 km MLS for SEAC^{4}RS storms. Outflow heights are typically 10-12 km MSL, but two cases had outflow heights at ~8 km MSL (Table S2). In some cases, the outflow measurement is taken downwind from the top of the updraft but within the storm anvil because the aircraft did not fly into the cloud top for safety reasons. The entrainment rate can be found through an iterative process by integrating the equation, every 1 km, from cloud base to cloud top. When the cloud-top mixing ratio (C_{top}) of the passive trace gas determined by the equation equals the aircraft-measured cloud-top passive trace gas mixing ratio (C_{meas}), the entrainment rate is found. Using the same analysis scripts by Barth et al. (2016), *n*-butane, *i*-butane, *n*-pentane, and *i*-pentane are used as the passive trace gases for most DC3 storms. These non-methane hydrocarbons have similarly shaped vertical profiles, which give consistent estimates of entrainment rate. The average entrainment rate derived from the four non-methane hydrocarbons is used to calculate the scavenging efficiency. For the 2 June 2012 case, CO is used as the passive trace gas. For the SEAC^{4}RS storms, the passive trace gases employed are from Cuchiara et al. (2020) and Cuchiara et al. (2023). CO and CO_2 are the passive trace gases for the 2 September 2013 storms, while CO_2 is the passive trace gas for the 18 September 2013 storms. More details on the entrainment rate calculations are given in Barth et al. (2016), Fried et al. (2016), Cuchiara et al. (2020), and Cuchiara et al. (2023).

https://doi.org/10.5194/egusphere-2025-6552
Preprint. Discussion started: 23 January 2026

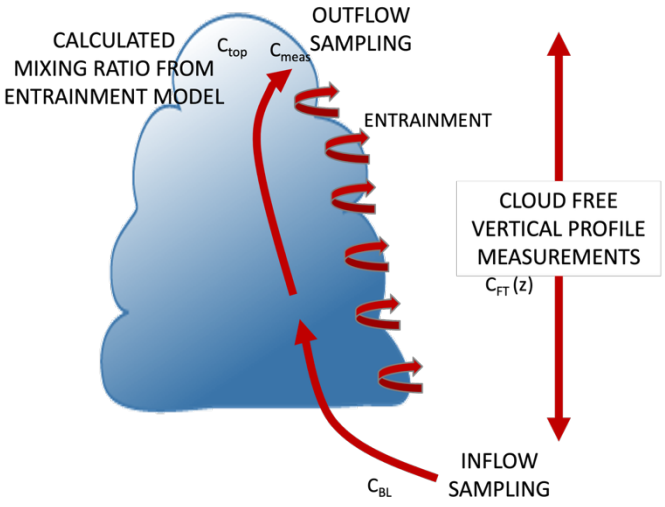

Figure 1. Schematic of airflow in a convective storm and sampling regions of the aircraft measurements to illustrate how the entrainment rate calculation is determined. C_{BL}, $C_{FT}(z)$, and C_{meas} are aircraft sampled mixing ratios in the boundary layer, free troposphere, and upper troposphere outflow, respectively. C_{top} is the cloud top mixing ratio calculated by the entrainment model. The turbulence in the convection creates mixing throughout the width of the cloud.

Using the calculated entrainment rate (Table S2), the same equation can be applied to each aerosol species, Y, to determine their concentrations at the cloud top if only transport and entrainment affected the concentration. The scavenging efficiency (SE, %) of the aerosol species is determined by simply subtracting the measured concentration of the aerosol species (Y_{meas}) from the calculated cloud-top aerosol concentration (Y_{top}) determined by the entrainment model and dividing by the calculated cloud-top value (Y_{top}):

$$SE = 100 \times \frac{Y_{top} - Y_{meas}}{Y_{top}} \quad (2)$$

The inflow and outflow time periods, listed in Table S2, were identified previously by Barth et al. (2016) and Cuchiara et al. (2020; 2023). The inflow and outflow regions are identified from flight segments in proximity to the radar reflectivity data. For the inflow region, the aircraft horizontal wind direction are used to confirm that sampled BL air is flowing towards the storm, while outflow time periods are determined by the horizontal winds, chemical signatures of hydrocarbons and CO, and ice water content (IWC). Concentrations of SO_4^{2-}, NH_4^+, pNO_3, and OA measured by the AMS in the inflow and outflow regions are provided in Table S3. To ensure that the inflow and outflow time periods are connected, our previous work (Barth et al., 2016, Fried et al., 2016, Cuchiara et al., 2020, and Cuchiara et al., 2023) used ratios of *i*- to *n*-butane and *i*- to *n*-pentane to confirm that the ratios did not change substantially.

https://doi.org/10.5194/egusphere-2025-6552
Preprint. Discussion started: 23 January 2026

The clear air vertical profiles are found by filtering the aircraft data to liquid plus ice water content < 0.001 g kg^{-1}, O_3/CO < 1.25 (to remove stratospheric air mixing into the troposphere), and a latitude-longitude region near the storm. In some storm cases, a time period is also specified to ensure the background air was near the storm of interest or remove impacts of smoke plumes also sampled by the plane but not ingested by the storm.

This observational analysis methodology has successfully been used in our previous studies (Barth et al., 2016; Fried et al., 2016; Cuchiara et al., 2020; Cuchiara et al., 2023), but for determining scavenging efficiencies of formaldehyde, hydrogen peroxide, and methyl hydrogen peroxide. Uncertainties in this approach for calculating scavenging efficiencies arise when other processes affect the aerosol concentration. Production of sulfate and oxalate via aqueous-phase chemistry can lead to higher sulfate and organic aerosol mass concentrations in the outflow region resulting in a lower scavenging efficiency estimate. Production of NO_x from lightning will subsequently form HNO_3 that partitions onto the aerosols, increasing NO_3^- aerosol mass concentrations in the outflow region and reducing NO_3^- and pNO_3 scavenging efficiency estimates. In addition, the entrainment model relies on vertical profiles of the background air to have a similar shape as that of the passive tracer used to determine the entrainment rate. If the aerosol vertical profile exhibits an anomalous enhancement in the mid to upper troposphere, then the aerosol scavenging efficiency estimate can be reduced because of entraining higher aerosol concentrations. When presenting the scavenging efficiency results below, these other processes are discussed.

4 Cloud chemistry parcel model

A prescribed cloud parcel model with gas and aqueous phase chemistry, described in Cuchiara et al. (2020), is used to examine the potential role of other processes on trace gas mixing ratios at cloud top. The cloud chemistry parcel model calculations focus only on the chemical transformations and do not interact with the entrainment model described above. Thus, the cloud chemistry parcel model calculations provide an indication of how much trace gas mixing ratios are altered, which, in turn, affect the aerosol concentrations in the convective outflow and the estimated aerosol scavenging efficiencies. The simulation and analyses are performed for only the 2 September 2013 SEAC^{4}RS case (Cuchiara et al., 2020), for which additional information from a WRF-chem can be used. The parcel model uses prescribed liquid water content, temperature, and air density that are taken from a WRF-Chem simulation (Cuchiara et al., 2020). The parcel model simulation begins at 15:00 local time and at an altitude of 1.2 km mean sea level (MSL; p = 883 hPa, T = 295.8 K) and spins up the gas-phase chemistry at this location for a 10-minute period so that short-lived oxidants (e.g., OH and HO_2) have typical concentrations. The parcel is then lofted at a constant vertical velocity until 11.5 km MSL. Initial gas-phase mixing ratios are taken from the observed 2 September 2013 BL mixing ratios (Cuchiara et al., 2020) or from WRF-Chem predicted values when observations are not available. A constant "lightning-generated" emission source of NO is applied between 262.15 K and 233.15 K so that ~1 ppbv NO_x is produced at cloud top, matching the 0.8-1.2 ppbv average enhanced NO_x sampled for this storm. The parcel model is run with two different assumed lightning-produced NO (LNO) emission profiles. For a constant updraft of 5 and 2 m s^{-1}, LNO emissions are set to 15 and 8 pptv per 10-second time step, respectively. The gas and aqueous

https://doi.org/10.5194/egusphere-2025-6552
Preprint. Discussion started: 23 January 2026

chemistry in the parcel model (Li et al., 2017; Barth et al., 2021) reasonably represents organic acid formation compared to other cloud chemistry models for a relatively clean rural location (Barth et al., 2021). The chemistry mechanism does not include any gas-phase production of organic acids, only aqueous-phase chemistry involving oxidation of dissolved aldehydes by OH. While formic acid (HCOOH) and acetic acid (CH_3COOH) have initial gas-phase mixing ratios of 565 pptv and 224 pptv, respectively, the other organic acids (acetic acid, glycolic acid, glyoxylic acid, pyruvic acid, and oxalic acid) are zero at the initial time.

5 Description of the case studies

As noted in Section 3, analyses of several storms observed during DC3 and SEAC^{4}RS have already been performed for trace gas wet removal (Barth et al., 2016; Fried et al., 2016; Bela et al., 2016, 2018; Cuchiara et al., 2020; Cuchiara et al., 2023). Here and in the supplement, we summarize the characteristics of these storms per these previous studies, to provide a sense of the range of conditions and variability of the storms studied. Scavenging efficiencies are calculated for four storms in the northeast Colorado – southwest Nebraska region and two storms in Oklahoma during DC3 (Table 1; Text S1). For SEAC^{4}RS, the analysis is performed for two storms sampled in Mississippi on 2 September 2013 and two storms sampled on 18 September 2013, one over the Gulf of Mexico and the other south of San Antonio, Texas. The storms differ in type, ranging from airmass to multicell to severe supercell storms. The maximum column radar reflectivity (Fig. S1) during the outflow time periods gives a sense of the storm severity along with the maximum height of the 20 dBZ reflectivity and the severe weather threat (SWEAT) index (Table 1). The SWEAT index, which combines low-level moisture, instability, wind speeds, and warm air advection using values at 850 hPa and 500 hPa, is often used by weather forecasters to predict the potential for severe storms (NWS Environmental Parameters and Indices, 2025). A SWEAT index >300 indicates the potential for severe convection that could cause damaging winds and hail, while a SWEAT index >400 indicates the potential for tornado formation. The SWEAT Index for each storm is calculated from radiosonde data. For DC3 storms, the sondes launched near the time and location of the storm as part of the field campaign are used for all cases except for 18 May 2012, which used the North Platte, Nebraska 0000 UTC 19 May 2012 radiosonde that was launched and located near the sampled storm. For the SEAC^{4}RS cases, aircraft vertical profiles in the storm vicinities are analyzed to determine the SWEAT index because the NWS routine radiosondes occurred several hours before the storms formed. Storm characteristics, anthropogenic and biogenic volatile organic compound (VOC) BL signatures, BL OA fraction (*f(OA)*), and aerosol dry extinction measured at 532 nm wavelength of these cases are summarized in the supplement for each case (Barth et al., 2015). The PM_1 is based on the AMS inorganic and organic aerosol plus the SP2 black carbon mass concentration, while *f(OA)* is the OA mass concentration divided by PM_1.

Table 1. Storm cases analyzed for aerosol mass concentration wet scavenging.

https://doi.org/10.5194/egusphere-2025-6552
Preprint. Discussion started: 23 January 2026

Date	Location	SWEAT Index[a]	Maximum Reflectivity (dBZ)	Maximum Height of 20 dBZ Level (km, MSL)
		DC3		
18 May 2012	SW Nebraska	283	58	14
29 May 2012	N Oklahoma	422	69	18
02 June 2012	NE Colorado	256	66	15
06 June 2012	NE Colorado	296	69	15
16 June 2012	Oklahoma	360	64	15
22 June 2012	SW Nebraska	442	72	18
		SEAC⁴RS		
02 Sept 2013	Mississippi	225	45	8
02 Sept 2013	Mississippi	209	55	13
18 Sept 2013	Gulf of Mexico	242	50	8
18 Sept 2013	Texas	257	46	8

[a]SWEAT Index = 12 [Td(850 hPa)] + 20 (TT - 49) + 2 (f8) + f5 + 125 (S + 0.2), where Td is the dewpoint temperature (°C) at 850 hPa, TT is the total totals index value (TT = T[850 hPa] + Td[850 hPa] – 2*T[500 hPa], where T is air temperature [°C]), f8 is the wind speed (kts) at 850 hPa, f5 is wind speed (kts) at 500 hPa, and S is the sine of the 500 hPa minus 850 hPa wind direction (NWS Environmental Parameters and Indices, 2025). Maximum NEXRAD reflectivity and heights of 20 dBZ levels are taken from the outflow time period of the aircraft sampling.

6 Clear air vertical profiles

Clear air vertical profiles of the aerosol mass concentrations are a key part of the analysis as they are used, along with the entrainment rate, to determine how much of the aerosol mass is transported to cloud top. For six out of the ten storms analyzed, the clear air vertical aerosol profiles exhibit typical shapes of high concentrations in the BL and low concentrations in the free troposphere (Fig. 2). The other four storms (18 May 2012, 2 June 2012, 6 June 2012, and 22 June 2012) show a mid-troposphere aerosol layer, most pronounced for pNO_3, in the mid-troposphere (Fig. 2a, c, d, f). The four storms with the mid-troposphere aerosol layer occurred in the northeast Colorado and southwest Nebraska region. For the 18 May case, many trace gases, including CO, HCN (a biomass burning tracer), SO_2, and HNO_3, do not show elevated mixing ratios in the mid-troposphere, but other trace gases or aerosol characteristics do. The measurements with higher values in the mid-troposphere layer include aerosol number concentration, surface area, and volume concentration, CO_2, OH, and peroxy nitrates. In the mid-troposphere layers, the pNO_3 partitioning is dominated by NO_3^- aerosol for all four storms (Fig. S2). Results from the E-AIM model in iterative mode show that the estimate of NH_3 gas-phase mixing ratios did not increase in these mid-troposphere layers. Both the observed and E-AIM predicted partitioning of NO_3^- strongly suggest that neither gradients in aerosol acidity nor meteorological factors can explain the large observed increases in inorganic aerosol nitrate in

https://doi.org/10.5194/egusphere-2025-6552
Preprint. Discussion started: 23 January 2026

the mid-troposphere layers, but that rather higher total inorganic nitrate (NO_3^- + HNO_3) is driving the shape of the altitude profiles.

The NOAA HYSPLIT model was used to generate back trajectories (Stein et al., 2015; Rolph et al., 2017) to understand potential source regions contributing to the mid-troposphere aerosol layers for the four cases in northeast Colorado and southwest Nebraska. The HYSPLIT back trajectories are initialized at aircraft locations where AMS pNO_3 concentrations are high compared to background values. The back trajectory calculations are driven by the North American Mesoscale (NAM) model reanalysis (Δx = 12 km) and run for 48 hours. For the 18 May, 6 June, and 22 June cases, several back trajectories are at low altitude (< 2 km AGL) in the central to southern Arizona region (Fig. S3), while the back trajectories for 2 June remain at mid-troposphere levels over the western US. On 2 June, the mid-troposphere aerosol layer may have arrived as outflow from convection upstream of the sampled storms, which are unlikely to be resolved by the NAM reanalysis. The back trajectories from the southwestern US are likely influenced by desert and agricultural emissions and possibly anthropogenic emissions from Phoenix, indicating that the air is being lofted from the desert southwest over the Rocky Mountains and remaining at the mid-troposphere altitudes.

No matter the source of the mid-troposphere aerosol layers, their elevated concentrations can impact the estimates of scavenging efficiencies due to entrainment of the high concentrations into the convection. The impact of the mid-troposphere aerosol layers is explored further in the next section by adjusting the clear-air vertical profiles for the four cases that had the mid-troposphere aerosol layers. Instead of using the measured clear air vertical profile, the vertical profile is adjusted to exclude the mid-troposphere layer (Fig. S4 exemplifies how this is done for the 18 May 2012 case). Using the entrainment model with the adjusted vertical profile, a new entrainment model predicted cloud top concentration is derived and used, together with the measured outflow concentration, to determine the scavenging efficiency by Eq. (2).

https://doi.org/10.5194/egusphere-2025-6552
Preprint. Discussion started: 23 January 2026

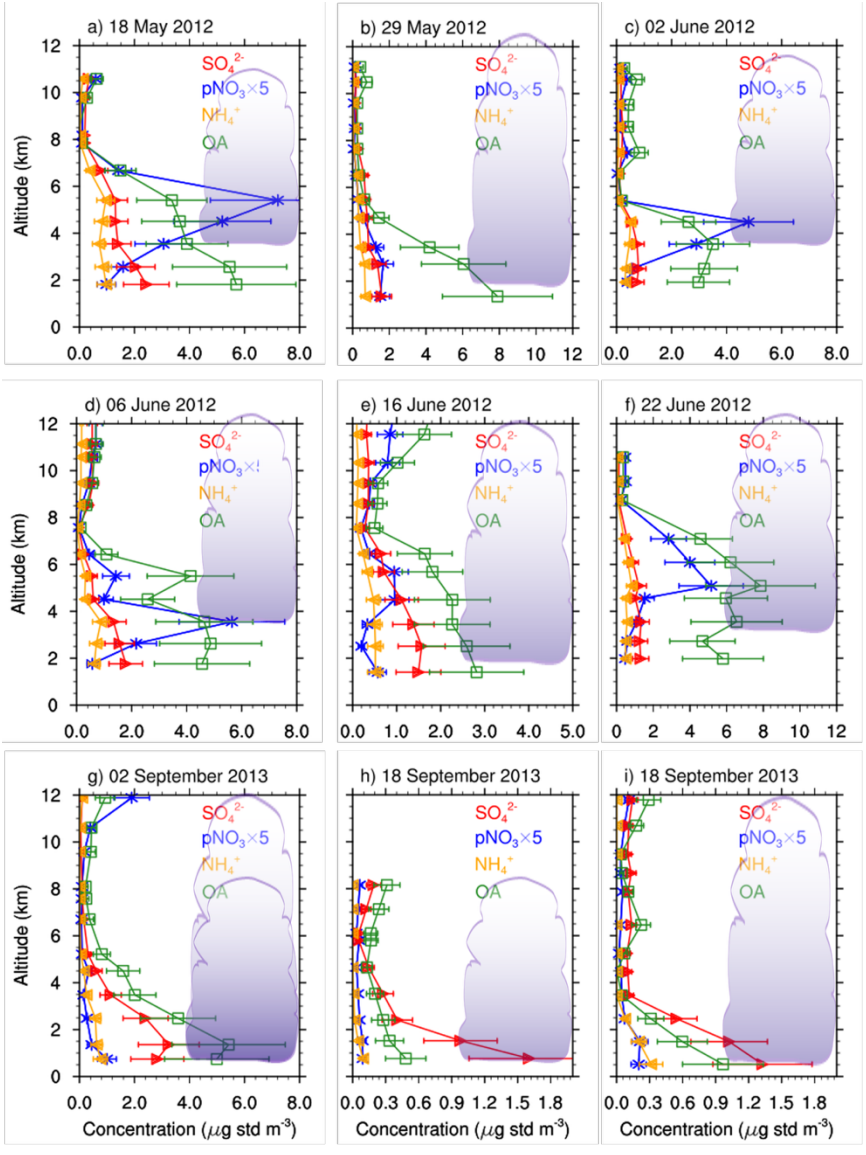

Figure 2. Clear air vertical profiles of sulfate (red with right arrows), nitrate (blue with asterisks), ammonium (gold with left arrows), and organic aerosol (green with squares) for a) 18 May 2012, b) 29 May 2012, c) 2 June 2012, d) 6 June 2012, e) 16 June 2012, f) 22 June 2012, g) 2 September 2013, h) 18 September 2013 over the Gulf of Mexico, and i) 18 September 2013 over South Texas. Average and standard deviations are plotted for each altitude bin, which is plotted at the average altitude of each 1-km bin. Nitrate concentrations shown are multiplied by a factor of 5 for visibility. The cloud schematic in each panel is used to locate the approximate cloud base and cloud top heights for each case. Cloud tops extending above the panel indicate that the actual cloud top was much greater than 12 km and is noted in Table 1. In g) two cloud tops are shown, ~8 km for the airmass storm and ~13 km for the multicell storm.

https://doi.org/10.5194/egusphere-2025-6552
Preprint. Discussion started: 23 January 2026

7 Aerosol scavenging efficiency

To visualize the aerosol mass scavenging efficiencies for the different convective storms, the average and standard deviation scavenging efficiencies are plotted in the parameter space of the SWEAT Index (Fig. 3), providing a way for understanding the scavenging efficiency results for different strengths of convection. Table S3 lists the measured aerosol mass concentrations in the inflow and outflow regions, the calculated aerosol mass concentration at cloud top, and the scavenging efficiency for each storm.

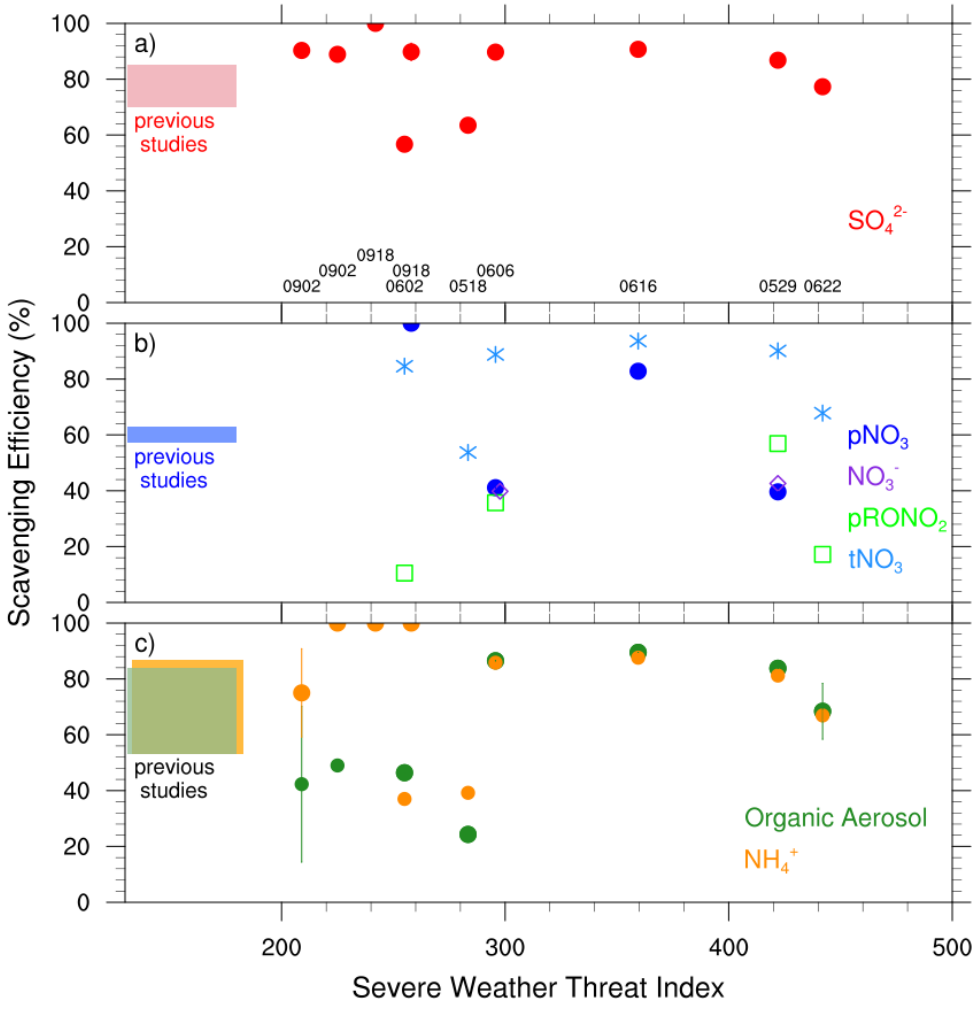

Figure 3. Scavenging efficiencies for a) sulfate, b) particulate nitrate (pNO_3; blue), and c) ammonium (orange), and organic (green) aerosol mass concentrations for DC3 and SEAC^{4}RS (filled circles) storms, plotted for each storm's SWEAT index. Scavenging efficiencies for inorganic particulate nitrate (NO_3^-), organic particulate nitrate ($pRONO_2$), and total nitrate (tNO_3 = pNO_3 + HNO_3) are shown in the middle panel as purple diamonds, green squares, and light blue asterisks, respectively. The error bars seen for the 22 June 2012 and 2 September 2013 cases are standard deviations of the scavenging efficiency

https://doi.org/10.5194/egusphere-2025-6552
Preprint. Discussion started: 23 January 2026

375 averaged over the multiple outflow intercepts. Dates (mmdd) of each storm are noted in black in panel a). Scavenging efficiencies from previous studies are shown for comparison but do not have corresponding SWEAT indices.

7.1 Sulfate aerosols

The scavenging efficiencies for SO_4^{2-} aerosol mass concentrations exceed 75% for all cases except two cases which give SO_4^{2-} scavenging efficiencies of 50-60% (Fig. 3). Obtaining fairly constant SO_4^{2-} scavenging efficiencies with different
380 storm severity points to the dominant role of in-cloud scavenging (i.e. cloud drop activation) and efficiency of producing precipitation in comparison to below-cloud scavenging. Previous studies have shown that SO_4^{2-} deposition fluxes and precipitation fluxes at the surface are positively correlated (e.g., Barth et al., 1992), which would suggest lower SO_4^{2-} scavenging efficiencies for weaker convective storms, in contrast to our findings of consistently high SO_4^{2-} scavenging. The high SO_4^{2-} aerosol scavenging efficiencies agree with other previous studies for convective clouds that found SO_4^{2-} aerosol
385 scavenging efficiencies of 70-86% (Hegg et al., 1984; Hilario et al., 2025; Yang et al., 2015). Yang et al. (2015) also analyzed the 29 May 2012 DC3 storm using a 4-layer entrainment model approach, which is similar to the analysis approach in this work. They found a SO_4^{2-} aerosol scavenging efficiency of 80-84% while our analysis determined 86.8% for that storm (Table S3). Hilario et al. (2025) estimated 87-95% SO_4^{2-} scavenging efficiencies for shallow to moderate tropical convection over the west Pacific. The two cases with 50-60% scavenging efficiencies are the 18 May and 2 June DC3 cases
390 that both had a significant mid-troposphere aerosol layer (Fig. 2). The SO_4^{2-} scavenging efficiency for the 22 June case, which also has an mid-troposphere aerosol layer, has a somewhat smaller value (77%) compared to the other severe deep convection cases. By adjusting the clear air vertical profile to remove the mid-troposphere aerosol layer, the aerosol SO_4^{2-} transported to cloud top is reduced by 0.06 μg std m^{-3} or less (where std m^{-3} refers to volume at T = 273 K and p = 1013 hPa) and scavenging efficiencies are within 3% of estimated values reported in Table S3. Thus, the mid-troposphere aerosol layer
395 does not substantially affect SO_4^{2-} scavenging efficiencies. Instead, other processes, such as aqueous phase production of SO_4^{2-}, could play a role.

7.2 Ammonium aerosols

The NH_4^+ aerosol scavenging efficiencies are >60% for most storms analyzed and 25-35% for the 18 May and 2 June DC3 storms (Fig. 3) which were influenced by the mid-troposphere aerosol layers (Fig. 2). Like SO_4^{2-} aerosol scavenging, the 22
400 June DC3 storm has a somewhat lower scavenging efficiency (67%) than the other severe storms. By adjusting the clear air vertical profile to remove the mid-troposphere aerosol layer, the NH_4^+ transported to cloud top is reduced by 0.06 μg std m^{-3} or less, reducing scavenging efficiencies because the denominator in Equation (1) is smaller. The fairly constant NH_4^+ scavenging efficiencies with different storm severity suggests that in-cloud scavenging is the dominant scavenging mechanism. Previous estimates of NH_4^+ aerosol scavenging efficiencies give a similar range (68-86%) as those calculated
405 here for most of the storms. Yang et al. (2015) found the NH_4^+ aerosol scavenging efficiency to be 80% for the 29 May 2012 storm using their 4-layer entrainment model approach, which is very similar to the 81.2% estimated here. For tropical,

https://doi.org/10.5194/egusphere-2025-6552
Preprint. Discussion started: 23 January 2026

oceanic convection, Hilario et al. (2025) estimated a wide range (54-87%) of NH_4^+ scavenging efficiencies. Note that the outflow NH_4^+ concentrations are near zero for some DC3 and SEAC^{4}RS storms (Table S3), which increases the relative uncertainty for those cases.

7.3 Nitrate aerosols

The estimated pNO_3 scavenging efficiencies shown in Fig. 3b (blue markers) are for only four of the ten storms analyzed. For two storms (16 June 2012 and 18 September 2013 land convection), pNO_3 scavenging efficiencies are > 80%, while the other two storms (6 June 2012 and 29 May 2012) have moderate pNO_3 scavenging efficiencies (~40%). The remaining six cases have indeterminate scavenging efficiencies because the outflow pNO_3 concentration is greater than the inflow concentration or the inflow and outflow concentrations are both below the detection limit (Table S3). Yang et al. (2015) found a moderate pNO_3 scavenging efficiency (57%) for the 29 May DC3 case that is lower than the SO_4^{2-} and NH_4^+ scavenging efficiencies yet still higher than the 39.6% determined in our analysis. The lower pNO_3 scavenging efficiencies are surprising because pNO_3 aerosols have hygroscopicity values similar to SO_4^{2-} and NH_4^+ and are often internally mixed with NH_4^+ and SO_4^{2-}. Thus, there are likely other processes causing higher outflow-to-inflow pNO_3 ratios relative to those for SO_4^{2-} and NH_4^+. Yang et al. (2015) suggested that outflow pNO_3 concentrations are likely affected by the partitioning between gas phase HNO_3 and pNO_3 in the higher acidity environment of the convective outflow. Their estimate of the total nitrate (tNO_3 = HNO_3 (g) + pNO_3) scavenging efficiency is 84%, supporting this idea. Our scavenging efficiency estimates of tNO_3 in the 29 May storm is 90% (Fig. 3, light blue markers) and >85% for other storms except the 18 May and 22 June DC3 storms . We note that the low altitude HNO_3 concentrations are a factor of 10 greater than pNO_3 and that HNO_3 does not exhibit a mid-troposphere enhancement (Fig. S2). These factors suggest our calculation of the combined scavenging efficiency is weighted toward the HNO_3 scavenging, which is >85%.

Employing the mass spectral marker method (Campuzano-Jost et al., 2021) to separate pNO_3 into inorganic (NO_3^-) and organic ($pRONO_2$) particulate nitrate and the E-AIM calculations (Section 2), the partitioning of inorganic nitrate between aerosol and gas phases is calculated, allowing us to quantify the NO_3^- fraction of NO_3^- + HNO_3. This fraction is small (<0.12) in DC3 inflow regions with NO_3^- concentrations <0.1 μg std m^{-3} (Table S4). In convective outflow regions the NO_3^- fraction increases substantially. The three cases where pNO_3 outflow concentrations are greater than its inflow concentrations have outflow NO_3^- fractions of 0.80-0.86. For both inflow and convective outflow regions, there is a positive correlation between the NO_3^- fraction and the pNO_3 concentration (Fig. S5). Scavenging efficiencies for NO_3^- and $pRONO_2$ are calculated only for storms where the inflow and outflow concentrations are at or above the detection limit. The scavenging efficiencies for NO_3^- match the pNO_3 values for the 6 June 2012 and 29 May 2012 storms (Fig. 3, purple diamonds; Table S5). The $pRONO_2$ scavenging efficiencies (Fig. 3, green squares) range from 11% to 57%. While the wide range of $pRONO_2$ scavenging efficiencies causes uncertainties in drawing conclusions, the similarity between NO_3^- and pNO_3 scavenging efficiencies suggest processes affecting NO_3^- are also affecting pNO_3 scavenging efficiencies.

https://doi.org/10.5194/egusphere-2025-6552
Preprint. Discussion started: 23 January 2026

Entrainment of the mid-troposphere aerosol layer increases the calculated cloud top aerosol concentration. Consequently, the mid-troposphere aerosol layer may alter the apparent aerosol scavenging efficiency. To quantify the increase in calculated cloud top pNO_3, the clear air vertical profile is adjusted to remove the mid-troposphere aerosol layer (Section 6). Without the mid-troposphere aerosol layer, the particulate nitrate transported to cloud top is reduced by 0.18 μg std m^{-3} for the 18 May case, a 64% decrease, and 0.06 μg std m^{-3} or less (30-55% decrease) for the other cases. For the 18 May, 2 June, and 22 June DC3 cases, the outflow pNO_3 concentrations are still greater than the transported cloud top pNO_3 concentrations. For the 6 June case, the lower transported cloud top concentration causes a smaller scavenging efficiency than that reported in Table S2 because the denominator in Equation (1) is also smaller.

Lightning production of nitrogen oxides could be a source of aerosol nitrate as the lightning-NO_x photochemically forms HNO_3, which partitions to aerosol nitrate. Using a chemistry-climate model, Tost et al. (2017) showed that lightning-NO_x increased nitrate aerosol concentrations by more than 50%, affecting aerosol size distributions and optical properties. Allen et al. (2012), using the CMAQ model, found that lightning-NO_x production increased the wet deposition of oxidized nitrogen. Here, we provide an example of production of HNO_3 from lightning-NO_x to determine the feasibility of this pathway in influencing the pNO_3 scavenging efficiency estimates. Results from a cloud chemistry parcel model that was used to examine the role of lightning-NO_x on formaldehyde and peroxide scavenging efficiencies (Cuchiara et al., 2020) are analyzed to estimate the production of HNO_3. This analysis is applied to the 2 September 2013 SEAC^{4}RS case, which had moderate lightning associated with the multicell storm. Two updrafts, 5 m s^{-1} and 2 m s^{-1}, are prescribed with two lightning-NO source strengths that produce ~1 ppbv of NO_x at the top of the cloud. In response to the added NO, the HNO_3 mixing ratio increases at cloud top by 100-200 pptv or 0.28-0.56 μg std m^{-3} (Fig. 4). This increase is larger than the 40 pptv increase of the sum of HNO_3 and pNO_3 during the 21 June 2012 convective outflow study reported by Nault et al. (2016), who highlighted the multiple inorganic and organic nitrate formation pathways occurring in convective outflow regions. The 100-200 pptv increase in HNO_3 from a lightning-NO source indicates that outflow particulate nitrate concentrations can potentially exceed the inflow concentrations as found in our analysis (Table S3). As it is not possible to properly represent lightning NO production in the cloud chemistry parcel model and HNO_3 partitioning onto aerosols, these results only indicate the potential pNO_3 increase. Chemistry transport modeling that represents cloud morphology and dynamics, lightning NO_x production, gas and aqueous phase chemistry, gas-phase HNO_3 partitioning onto ice, and gas-aerosol partitioning can be used in the future to further quantify the impact of lightning NO on pNO_3 in the upper troposphere.

https://doi.org/10.5194/egusphere-2025-6552
Preprint. Discussion started: 23 January 2026

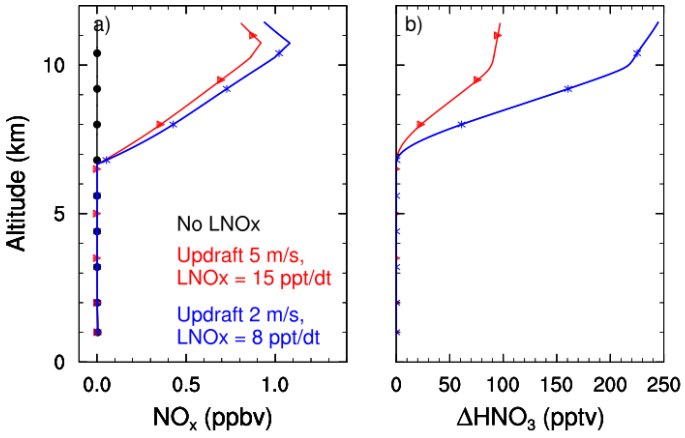

Figure 4. Results from the cloud chemistry parcel model of a) gas + aqueous NO_x mixing ratio and b) change in gas + aqueous HNO_3 mixing ratio caused by a lightning-NO_x source in the model. In a) the black line with filled circles is the NO_x mixing ratio without a lightning-NO_x source, while red with right triangles and blue with asterisks lines include a lightning-NO_x source using two different updraft speeds; a 20 pptv per 10-second time step of NO for the 5 m s^{-1} updraft and a 9 pptv per 10-second time step for the 2 m s^{-1} updraft. In b) the red line with right triangles is for the 20 pptv per 10-second time step lightning-NO_x source and 5 m s^{-1} updraft, while the blue with asterisks line is for 9 pptv per 10-second time step lightning-NO_x source and updraft 2 m s^{-1} speed.

7.4 Organic aerosols

The scavenging efficiencies for organic aerosol mass concentrations vary from 20-90% (Fig. 3). For SWEAT indices 300 and greater, the OA mass concentration scavenging efficiencies are similar to SO_4^{2-} and NH_4^+ scavenging efficiencies and indicate that OA is internally mixed with the more hygroscopic aerosols. Having OA internally mixed with the inorganic aerosols is supported by Schroder et al. (2018) who showed O/C ratios for DC3 and SEAC^{4}RS to be > 0.4 in their Fig. 4. Further, the severe storms have strong updrafts (>20 m s^{-1}) resulting in high supersaturations that activate most of the CCN to cloud drops.

The OA mass scavenging efficiencies in the less severe storms are <60%, suggesting other processes, such as aerosol or cloud chemistry, could be forming SOA resulting in higher OA concentrations in the convective outflow. While formation of SOA via aerosol chemistry can contribute, the presence of cloud drops through most of the depth of deep convection is a more likely SOA formation pathway. In liquid water, organic aerosol mass can increase from the aqueous phase OH oxidation of aldehydes and monocarboxylic acids to form dicarboxylic acids (Blando and Turpin, 2000; Ervens et al., 2011). Oxalic acid (HOOC-COOH) has been found to be the most abundant dicarboxylic acid in tropospheric aerosol particles (e.g., Kawamura and Sakaguchi, 1999; Ziemba et al., 2011). To assess the extent of aqueous processing, previous studies have used oxalate (the de-protonated form of oxalic acid) in combination with SO_4^{2-} for various regions (Hilario et al., 2021,

https://doi.org/10.5194/egusphere-2025-6552
Preprint. Discussion started: 23 January 2026

Sorooshian et al., 2007; Yu et al., 2005). Here, we use the same approach as Hilario et al. (2021) to evaluate the potential role of aqueous phase chemistry on OA mass concentrations in the convective outflow of the less severe storms.

Hilario et al. (2021) used the SAGA filter measurements of oxalate and SO_4^{2-} concentrations that in the analyzed datasets have a time resolution of 5 minutes or longer. For comparing oxalate to SO_4^{2-} ratios in convective outflow, this time resolution is much longer than the DC-8 aircraft sampling time in some cloud outflow regions (<40 seconds). Therefore, we use the 1-s AMS data for this analysis where the *m/*z 44 measurement represents oxalate or oxalic acid. This approximation is valid as oxalic acid has been shown to correlate strongly with and contribute a large fraction to *m/*z 44 (Takegawa et al., 2007) , with the rest of the signal being strongly impacted by other acids (Yatavelli et al., 2015). Furthermore, we compared all the SEAC^{4}RS oxalate to sulfate ratios from the SAGA measurements to the AMS *m/*z 44 to SO_4^{2-} ratios and found that the ratios have the same behavior for the two instruments in different types of air masses, indicating the AMS *m/*z 44 to SO_4^{2-} ratios can be used to look for signatures of cloud chemistry.

We first examine the *m/*z 44 to SO_4^{2-} ratios in different air mass regions for all SEAC^{4}RS flights. The UTLS region is for cloud free data (total water content < 0.001 g kg^{-1}) sampled above 8 km that also had HCN < 400 pptv and CH_3CN < 150 pptv to remove the influence from biomass burning (BB). The atmospheric BL region has the same criteria as the UTLS region, but for measurements sampled below 2 km altitude. Convective storm regions are where the DC-8 was sampling convective storms based on the flight descriptions in Toon et al. (2016) and with low HCN and CH_3CN mixing. BB regions are denoted by cloud free data with HCN > 400 pptv and CH_3CN > 150 pptv sampled near fires as described by Toon et al. (2016). Similar to Hilario et al. (2021) for oxalate to SO_4^{2-} ratios, the *m/*z 44 to SO_4^{2-} ratios for SEAC^{4}RS flights in BB air masses are higher than those without BB influences (Fig. 5). Measurements sampled near convection have higher *m/*z 44 to SO_4^{2-} ratios than those sampled in the BL. However, ratios in the UTLS have even higher *m/*z 44 to SO_4^{2-} ratios.

The 18 May 2012, 2 June 2012, 2 September 2013, and 18 September 2013 cases, which are the storms with OA scavenging efficiencies <60% and SWEAT indices < 300, are individually analyzed. The OA clear air vertical profiles (Fig. 2) do not exhibit a mid-troposphere layer, although the 2 June case does have a somewhat higher concentration (3.50 μg std m^{-3}) at 3.5 km altitude compared to the 2.97 μg std m^{-3} at 1.9 km altitude. The data are separated into BL, inflow, outflow, and cloud free regions (Fig. 5). All the cases have higher *m/*z 44 to SO_4^{2-} ratios in convective outflow air compared to the inflow air, except for the 18 May 2012 case, which has the same ratio in both air masses. The two SEAC^{4}RS convection cases sampled during midday show a substantial increase in *m/*z 44 to SO_4^{2-} ratios in the outflow region compared to the inflow and BL regions, as illustrated in Figs. 5e and 5f. The 18 May and 2 June 2012 DC3 convective storms have less of an influence of aqueous-phase chemistry, which may be because those storms were sampled during the late afternoon and early evening after the peak diurnal OH concentration and occurred in a low biogenic VOC environment.

https://doi.org/10.5194/egusphere-2025-6552
Preprint. Discussion started: 23 January 2026

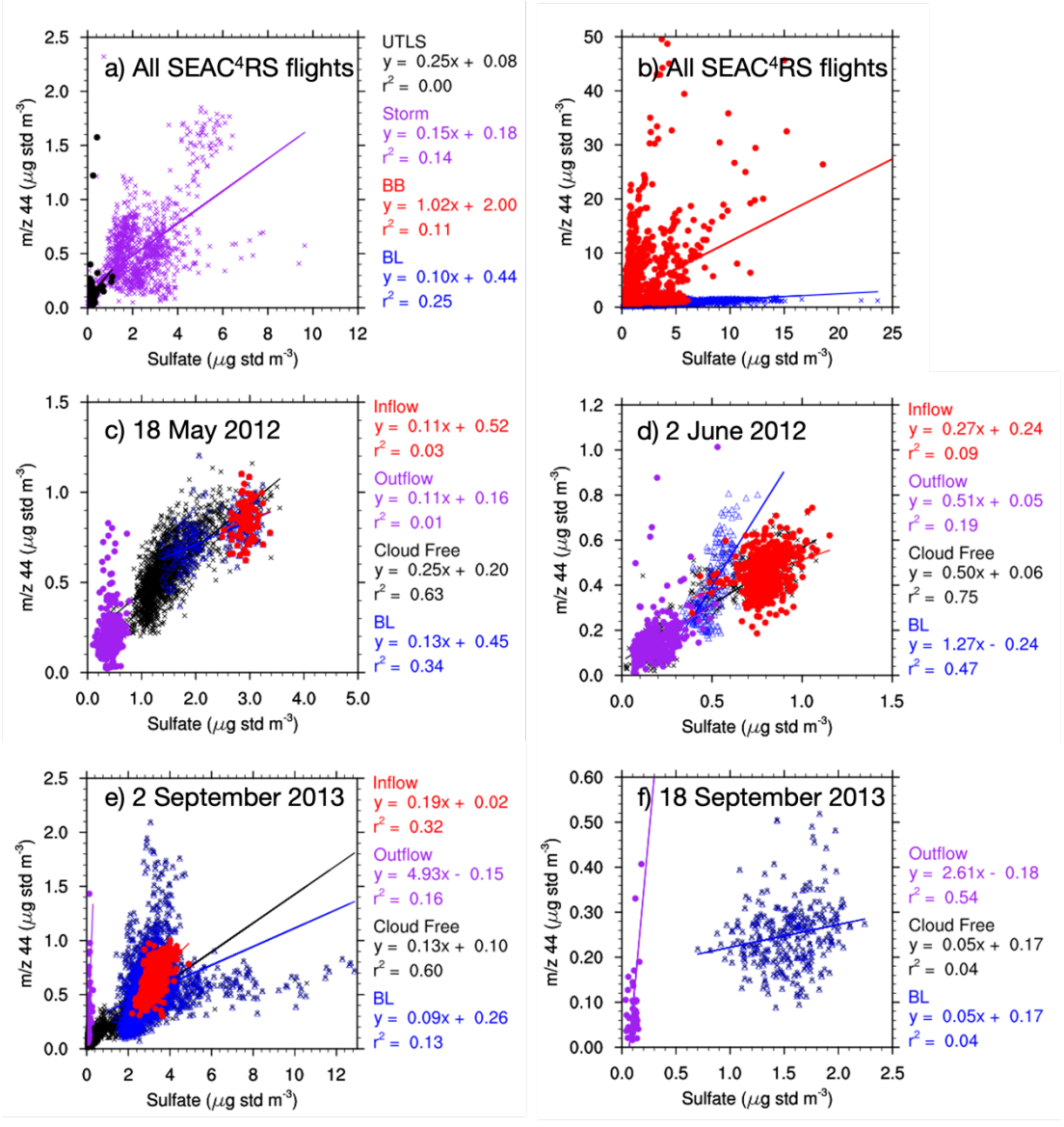

Figure 5. Scatter plots of AMS *m/z* 44 and AMS sulfate concentrations. In a) and b) concentrations from all the SEAC⁴RS flights are shown separating the data by region where a) shows cloud free UTLS data (black circles) at altitudes > 8 km and data near storms (purple crosses), and b) shows cloud free BL data (blue crosses) at altitudes < 2 km and data in BB regions (red circles). In panels c-f) data are separated by inflow (red), outflow (purple), cloud free (black), and BL regions (blue) as defined in the scavenging analysis (and BL data is below 2 km) for c) 18 May 2012, d) 2 June 2012, e) 2 September 2013, and f) 18 September 2013.

https://doi.org/10.5194/egusphere-2025-6552
Preprint. Discussion started: 23 January 2026

A second approach for investigating the role of aqueous-phase chemistry on OA concentrations in the convective outflow is to use the cloud chemistry parcel model described in Section 4 for the 2 September 2013 example case. For this discussion, the source of NO from lightning was set to zero, but results from the simulation with lightning-generated NO did not differ substantially. The liquid water content, prescribed by the WRF-Chem simulation (Cuchiara et al., 2020), shows a deep layer from 1.5 km MSL to 10 km MSL altitude with a peak value at 0.75 g kg^{-1} (Fig. 6a). Formic acid (HCOOH) is the predominant organic acid in both the aqueous phase and combined gas + aqueous phases (Fig. 6) for altitudes below 4 km. Near cloud base HCOOH and acetic acid (CH_3COOH) both rapidly form, while the other organic acids show a steady increase from just above cloud base to cloud top. At the top of the cloud, the estimated SOA mass concentration from the six organic acids is 1.79 µg C std m^{-3} and is 2.43 µg C std m^{-3} when glycolaldehyde, glyoxal, methylvinylketone, and hydoxyacetone are included in the summation, which is based on the particulate to gas phase partitioning ratios in the absence of clouds listed in Ervens et al. (2008). Of this total SOA estimate, 0.80 µg C std m^{-3} is from oxalic acid, which is more than the 0.40 µg std m^{-3} for the *m*/z 44 measurement in the outflow region of the 2 September case. Considering that the parcel model calculations predict higher SOA mass than the measured 1.5 µg OA std m^{-3} in the outflow of the 2 September 2013 multicell storm, it is quite likely that aqueous-phase chemistry contributed to higher outflow OA concentrations and thereby reducing the calculated OA scavenging efficiency for this storm. However, further investigation with CTMs of the contribution of organic aqueous phase chemistry to OA concentrations in individual convective storms is needed in order to represent the interactions between dynamics, physics, and chemistry more completely.

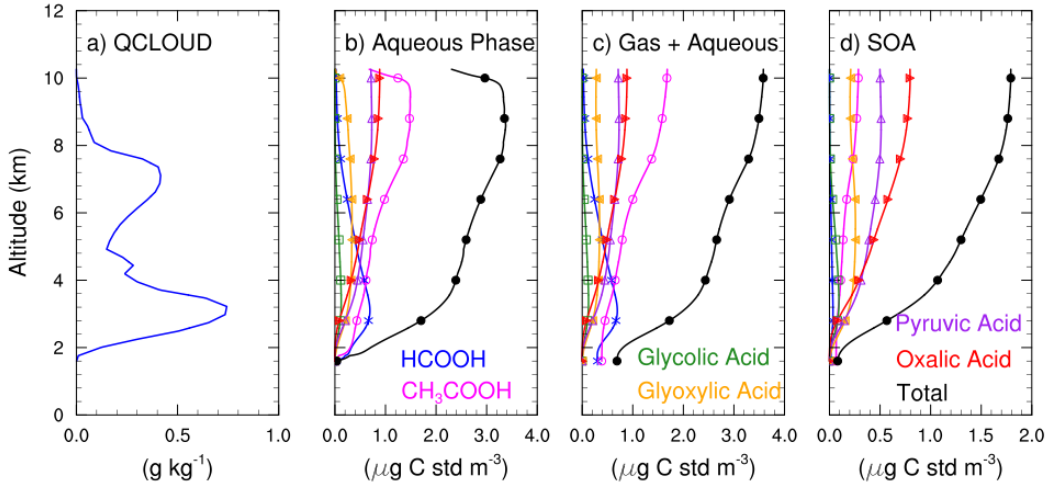

Figure 6. Prescribed cloud parcel model results for organic acid formation using the no lightning-NO_x scenario for the 2 September 2013 case. Panel a) shows the prescribed cloud water content (g kg^{-1}) for the model run, panel b) the aqueous-phase organic acid mixing ratios (µg C std m^{-3}), panel c) the total (gas + aqueous) organic acid mixing ratios (µg C std m^{-3}), and panel d) potential SOA (µg C std m^{-3}) using partitioning ratios, for formic acid (blue with asterisks), acetic acid

https://doi.org/10.5194/egusphere-2025-6552
Preprint. Discussion started: 23 January 2026

(magenta with open circles), glycolic acid (green with open square), glyoxylic acid (gold with left pointing triangles), pyruvic acid (purple with triangles), oxalic acid (red with right pointing triangles), and the sum of the six organic acids (black with closed circles).

8 Conclusions

This paper quantifies the vertical transport and scavenging of aerosol mass concentrations through analysis of ten deep convective storms observed during the 2012 DC3 and 2013 SEAC^{4}RS field campaigns. The storms sampled range in severity from weaker airmass convection to severe supercell convection. Similar to previous studies (Barth et al., 2016, Fried et al., 2016, Hilario et al., 2025, Yang et al., 2015), the analysis uses an entrainment model with input from aircraft measurements sampled in the inflow and outflow regions of the convective storms as well as clear-air vertical profiles to determine the scavenging efficiencies of sulfate, ammonium, nitrate, and organic aerosol mass concentrations.

The observationally derived scavenging efficiencies of sulfate and ammonium aerosol mass concentrations are consistently greater than 75% for weak to severe convection. The fairly constant scavenging efficiencies with different storm severity indicate that in-cloud scavenging is the dominant scavenging mechanism. The nitrate aerosol mass apparent scavenging efficiencies can be lower than the sulfate and ammonium scavenging efficiencies. For some storms the nitrate aerosol mass concentration in the outflow region of the storm is higher than its concentration in the air ingested by the storm in the BL. Examination of the clear air vertical profiles and their back trajectories suggest that entrainment of an elevated particulate nitrate mid-troposphere layer in some northeast Colorado / southwest Nebraska storms partially contribute to the higher nitrate concentrations in the outflow region. The production of NO_x from lightning followed by photochemical production of HNO_3 and its partitioning onto existing particles in the convective outflow can also contribute to higher particulate nitrate concentrations in the outflow region. A prescribed cloud parcel model with chemistry calculation shows that 100-200 pptv of HNO_3 (0.28-0.56 μg std m^{-3}) can be produced for ~1 ppbv NO emitted into the mid to upper updraft region of the cloud. While partitioning onto aerosols depends on the thermodynamic state, it is expected that this lightning-NO_x production is sufficient for explaining the high aerosol nitrate concentrations in several storms. To better quantify the influence of lightning-NO_x emissions on particulate nitrate concentrations in convective outflow regions, detailed cloud-scale chemistry transport modeling should be performed. The particulate organic nitrate scavenging efficiencies range from 11-57% for four DC3 storms with no obvious trend with storm severity, while particulate inorganic nitrate scavenging efficiencies for two DC3 storms are ~40% and match the total particulate nitrate scavenging for the two storms. In summary, the derived nitrate apparent scavenging efficiencies are influenced by entrainment and lightning-NO_x production with gas-aerosol partitioning, suggesting that chemistry transport models must represent these processes well within their convective schemes.

The observationally derived scavenging efficiencies for organic aerosol mass concentrations are greater than 60% in mostly severe storms and 20-50% in less severe storms. The DC3 storms in Colorado with elevated organic aerosol concentrations located in a mid-troposphere layer may have reduced the OA scavenging efficiencies. The SEAC^{4}RS storms consistently

https://doi.org/10.5194/egusphere-2025-6552
Preprint. Discussion started: 23 January 2026

have OA scavenging efficiencies < 50%. An explanation for the lower scavenging efficiencies is the aqueous-phase production of OA. The ratio of the AMS *m/z* 44 measurement can be used as a proxy for oxalate to sulfate as an indicator of cloud chemistry (Hilario et al., 2021). The higher *m/z* 44 to sulfate ratios found in the outflow region compared to the atmospheric boundary layer indicate that cloud chemistry likely affect the calculated scavenging efficiency. This is supported by the prescribed cloud parcel model with chemistry calculations that shows SOA mass from oxalic acid to be 0.8 μg C std m^{-3} and from the sum of semi-volatile organic compounds to be 2.4 μg C std m^{-3}. Thus, organic aerosol scavenging efficiencies can be influenced by cloud chemistry, suggesting that chemistry transport models should include organic aqueous-phase cloud chemistry production of aerosols.

Since scavenging of aerosols by clouds directly affects the aerosol concentrations and lifetime in the atmosphere, this important sink is critical for representing well in air quality and climate models because of the role aerosols have on human health and the atmosphere's energy balance. While it is especially difficult for regional and global scale models to represent the specific storm cases analyzed in this paper, connecting this analysis with a hierarchy of chemistry transport models, cloud scale to regional scale to global scale, is a way to utilize this detailed observational analysis. The results presented here can be used directly for evaluating cloud-scale chemistry transport model representation of aerosol scavenging. Then, the cloud-scale model results can be expanded to examine ratios of aerosol concentrations to trace gases that are primarily transported through convection. These ratios can then be evaluated in the regional and global scale chemistry transport models. This hierarchical modeling approach, which has not been performed in the past for scavenging studies as far as we know, should also benefit investigations of other chemistry and aerosols processes (e.g., aerosol-cloud interactions) occurring in clouds.

9 Code Availability

The Extended AIM (E-AIM) aerosol thermodynamics model is available at https://www.aim.env.uea.ac.uk/aim/aim.php.

The NCAR Command Language version 6.6.2 (2019) was used for the data analysis and is available at https://www.ncl.ucar.edu/. The cloud chemistry box model source code and input files are available upon request to the corresponding author. The AMATI package is available at https://gitlab.com/JimenezGroup/amati.

10 Data Availability

All data from the DC3 field project can be found at http://data.eol.ucar.edu/master_list/?project=DC3. Specifically, the DC3 and SEAC^{4}RS aircraft data are located at http://www-air.larc.nasa.gov/cgi-bin/ArcView/dc3-seac4rs and https://www-air.larc.nasa.gov/cgi-bin/ArcView/seac4rs, respectively. NWS radiosonde data are from the NOAA National Centers for Environmental Information and University of Wyoming archive (https://weather.uwyo.edu/upperair/sounding.shtml), respectively. Output from the reprocessed AMS data, NEXRAD composite radar data processed by GridRad, and the cloud

https://doi.org/10.5194/egusphere-2025-6552
Preprint. Discussion started: 23 January 2026

chemistry box model output are available from the Zenodo data repository (https://doi.org/10.5281/zenodo.18089619, Barth et al., 2025).

620

11 Supplement Link

12 Author Contribution

MB designed and carried out the analysis. PCJ and JLJ collected the AMS measurements, advised on the analysis method, and provided insight and interpretations of the measurements. GC and AP advised on the analysis method and interpretation
625 of the results. MRAH provided back-trajectory information and GL conducted the sulfate to oxalate analysis, both under the guidance of AS. MB prepared the manuscript with contributions from all co-authors.

13 Competing Interests

The authors declare that they have no conflict of interest. Armin Sorooshian is a member of the editorial board of the Atmospheric Chemistry and Physics journal.

630 **14 Acknowledgments**

The authors thank the DC3 and SEAC^{4}RS Science and Logistics teams for the successful execution of the two field campaigns. We thank Cameron Homeyer (University of Oklahoma) for processing the data from multiple radars, providing three-dimensional composites. We would like to acknowledge the use of the Casper system (https://ncar.pub/casper) supported by the NSF National Center for Atmospheric Research (NCAR) at the NSF NCAR-Wyoming Supercomputing
635 Center, sponsored by the National Science Foundation and the State of Wyoming. The authors very much appreciate the reviews of the paper by Behrooz Roozitalab and Warren Smith.

15 Financial Support

This material is based upon work supported by the NASA Atmospheric Composition Modeling and Analysis Program Award Number 80NSSC21K1347 and the NSF National Center for Atmospheric Research, which is a major facility
640 sponsored by the U.S. National Science Foundation under Cooperative Agreement No. 1852977. M. R. A. H. acknowledges support from the UCAR Next Generation Fellowship and the NSF NCAR Graduate Visitor Program. G.R.L acknowledges support from the NSF NCAR/ACOM Ralph Cicerone Fellowship.

https://doi.org/10.5194/egusphere-2025-6552
Preprint. Discussion started: 23 January 2026

16 References

Abdul-Razzak, H., and Ghan, S. J.: A parameterization of aerosol activation, 2, Multiple aerosol types, J. Geophys. Res., 105, 6837–6844, doi:10.1029/1999JD901161, 2000.

Allen, D. J., Pickering, K. E., Pinder, R. W., Henderson, B. H., Appel, K. W., and Prados, A.: Impact of lightning-NO on eastern United States photochemistry during the summer of 2006 as determined using the CMAQ model, Atmos. Chem. Phys., 12, 1737–1758, doi: 10.5194/acp-12-1737-2012, 2012.

Apel, E. C., Hornbrook, R. S., Hills, A. J., Blake, N. J., Barth, M. C., Weinheimer, A., Cantrell, C., Rutledge, S. A., Basarab, B., Crawford, J., Diskin, D., Homeyer, C. R., Campos, T., Flocke, F., Fried, A., Blake, D. R., Brune, W., Pollack, I., Peischl, J., Ryerson, T., Wennberg, P. O., Crounse, J. D., Wisthaler, A., Mikoviny, T., Huey, G., Heikes, B., O'Sullivan D., and Riemer, D. D.: Upper tropospheric ozone production from lightning NOx-impacted convection: Smoke ingestion case study from the DC3 campaign, J. Geophys. Res., 120, 2505– 2523, doi:10.1002/2014JD022121, 2015.

Barth, M. C., Hegg, D. A., and Hobbs, P. V.: Numerical modeling of cloud and precipitation chemistry associated with two rainbands and some comparisons with observations, J. Geophys. Res., 97, 5825–5845, doi:10.1029/92JD00464, 1992.

Barth, M. C., Cantrell, C. A., Brune, W. H., Rutledge, S. A., Crawford, J. H., Huntrieser, H., Carey, L. D., MacGorman, D., Weisman, M., Pickering, K. E., Bruning, E., Anderson, B., Apel, E., Biggerstaff, M., Campos, T., Campuzano-Jost, P., Cohen, R., Crounse, J., Day, D. A., Diskin, G., Flocke, F., Fried, A., Garland, C., Heikes, B., Honomichl, S., Hornbrook, R., Huey, L. G., Jimenez, J., Lang, T., Lichtenstern, M., Mikoviny, T., Nault, B., O'Sullivan, D., Pan, L., Peischl, J., Pollack, I., Richter, D., Riemer, D., Ryerson, T., Schlager, H., St. Clair, J., Walega, J., Weibring, P., Weinheimer, A., Wennberg, P., Wisthaler, A., Wooldridge, P., and Ziegler, C.: The Deep Convective Clouds and Chemistry (DC3) Field Campaign, Bull. Amer. Meteor. Soc., 96, 1281–1309, doi: 10.1175/BAMS-D-13-00290.1, 2015.

Barth, M. C., Bela, M. M., Fried, A., Wennberg, P., Crounse, J., St. Clair, J., Blake, N., Blake, D. R., Homeyer, C. R., Brune, W. H., Zhang, L., Mao, J., Ren, X., Ryerson, T., Pollack, I. B., Peischl, J., Cohen, R. C., Nault, B. A., Huey, L. G., Liu, X., and Cantrell, C. A.: Convective Transport and Scavenging of Peroxides by Thunderstorms Observed over the Central U.S. during DC3, J. Geophys. Res., 121, 4272– 4295, doi:10.1002/2015JD024570, 2016.

Barth, M. C., Ervens, B., Herrmann, H., Tilgner, A., McNeill, V. F., Tsui, W. G., Deguillaume, L., Chaumerliac, N., Carlton, A., and Lance, S. M.: Box model intercomparison of cloud chemistry, J. Geophys. Res., 126, doi:10.1029/2021JD035486, 2021.

Bela, M. M., Barth, M. C., Toon, O. B., Fried, A., Homeyer, C. R., Morrison, H., Cummings, K. A., Li, Y., Pickering, K. E., Allen, D., Yang, Q., Wennberg, P. O., Crounse, J. D., St. Clair, J. M., Teng, A. P., O'Sullivan, D., Huey, L. G., Chen, D., Liu, X., Blake, D., Blake, N., Apel, E., Hornbrock, R. S., Flocke, F., Campos, T., and Diskin, G.: Wet scavenging of

https://doi.org/10.5194/egusphere-2025-6552
Preprint. Discussion started: 23 January 2026

soluble species in DC3 deep convective storms using aircraft observations and WRF-Chem simulations, J. Geophys. Res., 121, 4233– 4257, doi:10.1002/2015JD024623, 2016.

Bela, M. M., Barth, M. C., Toon, O. B., Fried, A., Ziegler, C., Cummings, K. A., Li, Y., Pickering, K. E., Homeyer, C. R., Morrison, H., Yang, Q., Mecikalski, R. M., Carey, L., Biggerstaff, M. I., Betten, D. P., and Alford, A. A.: Effects of scavenging, entrainment, and aqueous chemistry on peroxides and formaldehyde in deep convective outflow over the central and Southeast U.S., J. Geophys. Res., 123, 7594– 7614, doi: 10.1029/2018JD028271, 2018.

Blando, J. D., and Turpin, B. J.: Secondary organic aerosol formation in cloud and fog droplets: A literature evaluation of plausibility. Atmos. Environ., 34(10), 1623–1632, doi:10.1016/S1352-2310(99)00392-1, 2000.

Borbon, A., Ruiz, M., Bechara, J., Aumont, B., Chong, M., Huntrieser, H., Mari, C., Reeves, C. E., Scialom, G., Hamburger, T., Stark, H.., Afif, C., Jambert, C. Mills, G., Schlager, H. and Perros, P. E.: Transport and chemistry of formaldehyde by mesoscale convective systems in West Africa during AMMA 2006, J. Geophys. Res., 117, D12301, doi:10.1029/2011JD017121, 2012.

Campuzano-Jost, P., Sueper, D. S., Clegg, S. L., Nault, B., Guo, H., and Jimenez, J. L.: Introducing AMATI, a new tool for rapid aerosol thermodynamic calculations on large field datasets, AGU Fall Meeting 2021, New Orleans, Louisiana, USA, 13-17 December 2021, A45X-2177, https://agu.confex.com/agu/fm21/meetingapp.cgi/Paper/983500, 2021.

Canagaratna, M. R., Jayne, J. T., Jimenez, J. L., Allan, J. D., Alfarra, M. R., Zhang, Q., Onasch, T. B., Drewnick, F., Coe, H., Middlebrook, A., Delia, A., Williams, L. R., Trimborn, A. M., Northway, M. J., DeCarlo, P. F., Kolb, C. E., Davidovits, P., and Worsnop, D. R.: Chemical and microphysical characterization of ambient aerosols with the Aerodyne aerosol mass spectrometer, Mass Spectrom. Rev., 26, 185–222, doi:10.1002/mas.20115, 2007.

Chen, Y., Xu, L., Humphry, T., Hettiyadura, A. P. S., Ovadnevaite, J., Huang, S., Poulain, L., Schroder, J. C., Campuzano-Jost, P., Jimenez, J. L., Herrmann, H., O'Dowd, C., Stone, E. A., and Ng, N. L.: Response of the Aerodyne aerosol mass spectrometer to inorganic sulfates and organosulfur compounds: Applications in field and laboratory measurements, Environ. Sci. Technol., 53, 5176–5186, doi:10.1021/acs.est.9b00884 2019.

Clegg, S. L., Brimblecombe, P., and Wexler, A. S.: Thermodynamic model of the system H^+–NH_4^+–SO_4^{2-}–NO_3^-–H_2O at tropospheric temperatures, J. Phys. Chem. A, 102, 2137–2154, doi: 10.1021/jp973043j, 1998.

Cohan, D. S., Schultz, M. G., Jacob, D. J., Heikes, B. G. and Blake, D. R.: Convective injection and photochemical decay of peroxides in the tropical upper troposphere: Methyl iodide as a tracer of marine convection, J. Geophys. Res., 104, 5717–5724, doi:10.1029/98JD01963, 1999.

Croft, B., Lohmann, U., Martin, R. V., Stier, P., Wurzler, S., Feichter, J., Posselt, R., and Ferrachat, S.: Aerosol size-dependent below-cloud scavenging by rain and snow in the ECHAM5-HAM, Atmos. Chem. Phys., 9, 4653–4675, doi: 10.5194/acp-9-4653-2009, 2009.

https://doi.org/10.5194/egusphere-2025-6552
Preprint. Discussion started: 23 January 2026

Cuchiara, G. C., Fried, A., Barth, M. C., Bela, M., Homeyer, C. R., Gaubert, B., Walega, J., Weibring, P., Richter, D., Wennberg, P., Crounse, J., Kim, M., Diskin, G., Hanisco, T. M., Wolfe, G. M., Beyersdorf, A., Peischl, J., Pollack, I. B., St. Clair, J. M., Woods, S., Tanelli, S., Bui, T. P., Dean-Day, J., Huey, G. L., and Heath, N.: Vertical transport, entrainment, and scavenging processes affecting trace gases in a modeled and observed SEAC^{4}RS case study. J. Geophys. Res., 125, e2019JD031957, doi.org/10.1029/2019JD031957, 2020.

Cuchiara, G. C., Fried, A., Barth, M. C., Bela, M., Homeyer, C. R., Walega, J., Weibring, P., Richter, D., Woods, S., Beyersdorf, A., Bui, T. P., Dean-Day, J.: Effect of marine and land convection on wet scavenging of ozone precursors observed during a SEAC^{4}RS case study, J. Geophys. Res., 28, e2022JD037107, doi.org/10.1029/2022JD037107, 2023.

Day, D. A., Campuzano-Jost, P., Nault, B. A., Palm, B. B., Hu, W., Guo, H., Wooldridge, P. J., Cohen, R. C., Docherty, K. S., Huffman, J. A., de Sá, S. S., Martin, S. T., and Jimenez, J. L.: A systematic re-evaluation of methods for quantification of bulk particle-phase organic nitrates using real-time aerosol mass spectrometry, Atmos. Meas. Tech., 15, 459–483, doi:10.5194/amt-15-459-2022, 2022.

DeCarlo, P., Kimmel, J., Trimborn, A., Northway, M., Jayne, J., Aiken, A., Gonin, M., Fuhrer, K., Horvath, T., Docherty, K., Worsnop, D., and Jimenez, J.: Field-deployable, high-resolution, time-of-flight aerosol mass spectrometer, Anal. Chem., 78, 8281–8289, doi:10.1021/ac061249n, 2006.

Dibb, J. E., Talbot, R. W., Scheuer, E. M., Seid, G., Avery, M. A., and Singh, H. B.: Aerosol chemical composition in Asian continental outflow during the TRACE-P campaign: Comparison with PEM-West B, J. Geophys. Res., 108, 8815–8815, doi:10.1029/2002JD003111, 2003.

Dickerson, R. R., Huffman, G. J., Luke, W. T., Nunnermacker, L. J., Pickering, K. E., Leslie, A. C. D., Lindsey, C. G., Slinn, W. G. N., Kelly, T. J., Daum, P. H., Delany, A. C., Greenberg, J. P., Zimmerman, P. R., Boatman, J. F., Ray, J. D., and Stedman, D. H.: Thunderstorms: An important mechanism in the transport of air pollutants, Science, 235, 460–465, doi:10.1126/science.235.4787.460, 1987.

DiGangi, E. A., MacGorman, D. R., Ziegler, C. L., Betten, D., Biggerstaff, M., Bowlan, M., and Potvin, C. K.: An overview of the 29 May 2012 Kingfisher supercell during DC3, J. Geophys. Res. Atmos., 121, 14,316–14,343, doi:10.1002/2016JD025690, 2016.

Ervens, B., Carlton, A. G., Turpin, B. J., Altieri, K. E., Kreidenweis, S. M., and Feingold, G.: Secondary organic aerosol yields from cloud-processing of isoprene oxidation products, Geophys. Res. Lett., 35, L02816, doi:10.1029/2007GL031828, 2008.

Ervens, B., Turpin, B. J., and Weber, R. J.: Secondary organic aerosol formation in cloud droplets and aqueous particles (aqSOA): A review of laboratory, field and model studies. Atmos. Chem. and Phys., 11(21), 11069–11102, doi:10.5194/acp-11-11069-2011, 2011.

https://doi.org/10.5194/egusphere-2025-6552
Preprint. Discussion started: 23 January 2026

Farmer, D. K., Matsunaga, A., Docherty, K. S., Surratt, J. D., Seinfeld, J. H., Ziemann, P. J., and Jimenez, J. L.: Response of an aerosol mass spectrometer to organonitrates and organosulfates and implications for atmospheric chemistry, Proc. Natl. Acad. Sci. U. S. A., 107, 6670–6675, doi:10.1073/pnas.0912340107, 2010.

Flossmann, A. I., Hall, W. D. and Pruppacher, H. R.: A theoretical study of the wet removal of atmospheric pollutants. Part I: The redistribution of aerosol particles captured through nucleation and impaction scavenging by growing cloud drops. J. Atmos. Sci., 42, 583–606, doi:/10.1175/1520-0469(1985)042<0583:ATSOTW>2.0.CO;2, 1985.

Fried, A., Barth, M. C., Bela, M., Weibring, P., Richter, D., Walega, J., Li, Y., Pickering, K. E., Apel, E., Hornbrock, R. S., Hills, A., Riemer, D. D., Blake, N., Blake, D., Schroeder, J. R., Luo, Z. J., Crawford, J. H., Olson, J., Rutledge, S., Betten, D., Biggerstaff, M. I., Diskin, G., Sachse, G., Campos, T., Flocke, F., Weinheimer, A., Cantrell, C., Pollack, I., Peischl, J., Froyd, K., Wisthaler, A., Mikoviny, T. and Woods, S.: Convective Transport of formaldehyde to the upper troposphere and lower stratosphere and associated scavenging in thunderstorms over the Central United States during the 2012 DC3 study, J. Geophys. Res., 120, 7430– 7460, doi:10.1002/2015JD024477, 2016.

Friese, E. and Ebel, A.: Temperature dependent thermodynamic model of the system H^+–NH_4^+–Na^+–SO_4^{2-}–NO_3^-–Cl^-–H_2O, J. Phys. Chem. A, 114, 11595–11631, doi:10.1021/jp101041j, 2010.

Gong, W., Stroud, C., and Zhang, L.: Cloud processing of gases and aerosols in air quality modeling, Atmosphere, 2, 567–616, doi:10.3390/atmos2040567, doi:10.3390/atmos2040567, 2011.

Guo, H., Sullivan, A. P., Campuzano-Jost, P., Schroder, J. C., Lopez-Hilfiker, F. D., Dibb, J. E., Jimenez, J. L., Thornton, J. A., Brown, S. S., Nenes, A., and Weber, R. J.: Fine particle pH and the partitioning of nitric acid during winter in the northeastern United States, J. Geophys. Res., 121, 500, doi:10.1002/2016JD025311, 2016.

Guo, H., Campuzano-Jost, P., Nault, B. A., Day, D. A., Schroder, J. C., Kim, D., Dibb, J. E., Dollner, M., Weinzierl, B., and Jimenez, J. L.: The importance of size ranges in aerosol instrument intercomparisons: A case study for the Atmospheric Tomography Mission, Atmos. Meas. Tech., 14, 3631–3655, doi:10.5194/amt-14-3631-2021, 2021.

Hegg, D. A. and Hobbs, P. V.: Cloud water chemistry and the production of sulfates in clouds, Atmos. Environ., 15, 1597-1604, doi:10.1016/0004-6981(81)90144-X, 1981.

Hegg, D. A. and Hobbs, P. V.: Measurements of sulfate production in natural clouds, Atmos. Environ., 16, 2663-2668, doi:10.1016/0004-6981(82)90348-1, 1982.

Hegg, D. A., Hobbs, P. V., and Radke, L. F.: Measurements of the scavenging of sulfate and nitrate in clouds, Atmos. Environ., 18, 1939-1946, doi:10.1016/0004-6981(84)90371-8, 1984.

Herndon, R.: “Storm Data and Unusual Weather Phenomena”, National Climatic Data Center, 54, (5), 2012a.

Herndon, R.: “Storm Data and Unusual Weather Phenomena”, National Climatic Data Center, 54, (6), 2012b.

https://doi.org/10.5194/egusphere-2025-6552
Preprint. Discussion started: 23 January 2026

Hilario, M. R. A., Crosbie, E., Bañaga, P. A., Betito, G., Braun, R. A., Cambaliza, M. O., Corral, A. F., Cruz, M. T., Dibb, J., Lorenzo, G. R., MacDonald, A. B., Robinson, C. E., Shook, M. A., Simpas, J. B., Stahl, C., Winstead, E., Ziemba, L., and Sorooshian, A.: Particulate oxalate-to-sulfate ratio as an aqueous processing marker: Similarity across field campaigns and limitations. Geophysical Research Letters, 48, e2021GL096520. doi: 10.1029/2021GL096520, 2021.

Hilario, M. R. A., Barth, M., Bennett, R., Crosbie, E., DiGangi, J. P., Diskin, G. S., Lorenzo, G. R., Rutledge, S., Martin, M. Y., Ziemba, L. and Sorooshian, A.: Quantifying scavenging efficiencies of different aerosol species and size-resolved volume concentrations in tropical convective clouds over the West Pacific, J. Atmos. Sci., 82, 267–282, doi:10.1175/JAS-D-24-0064.1, 2025.

Homeyer, C. R. and Bowman, K. P.: Algorithm description document for version 3.1 of the three-dimensional gridded NEXRAD WSR-88D radar (GridRad). [Dataset Technical Report]. University of Oklahoma. http://gridrad.org/pdf/GridRad-v3.1-Algorithm-Description.pdf, 2017 [last accessed: 11 August 2025]

IPCC: Climate Change 2021: The Physical Science Basis. Contribution of Working Group I to the Sixth Assessment Report of the Intergovernmental Panel on Climate Change [Masson-Delmotte, V., P. Zhai, A. Pirani, S.L. Connors, C. Péan, S. Berger, N. Caud, Y. Chen, L. Goldfarb, M.I. Gomis, M. Huang, K. Leitzell, E. Lonnoy, J.B.R. Matthews, T.K. Maycock, T. Waterfield, O. Yelekçi, R. Yu, and B. Zhou (eds.)]. Cambridge University Press, Cambridge, United Kingdom and New York, NY, USA, 2391 pp. doi:10.1017/9781009157896, 2021.

Jensen, J. B. and Charlson, R. J.: On the efficiency of nucleation scavenging, Tellus B, 36B, 367–375, doi:10.1111/j.1600-0889.1984.tb00255.x, 1984.

Jones, A. C., Hill, A., Hemmings, J., Lemaitre, P., Quérel, A., Ryder, C. L., and Woodward, S.: Below-cloud scavenging of aerosol by rain: A review of numerical modelling approaches and sensitivity simulations with mineral dust in the Met Office's Unified Model, Atmos. Chem. Phys., 22, 11381–11407, doi: 10.5194/acp-22-11381-2022, 2022.

Kawamura, K. and Sakaguchi, F.: Molecular distributions of water soluble dicarboxylic acids in marine aerosols over the Pacific Ocean including tropics, J. Geophys. Res., 104(D3), 3501–3509, doi:10.1029/1998JD100041, 1999.

Lawrence, C., Barth, M., Orlando, J., Casson, P., Brandt, R., Kelting, D., Yerger, E., and Lance, S.: Process analysis of elevated concentrations of organic acids at Whiteface Mountain, New York, Atmos. Chem. Phys., 24, 13693–13713, doi:10.5194/acp-24-13693-2024, 2024.

Li, E., Pierce, J. R., Juncosa Calahorrano, J. F., Sullivan, A. P., Pollack, I. B., Roscioli, J. R., Caulton, D. R., McCabe, M. E., Jathar, S. H., Fischer, E. V.: Inorganic nitrogen gas-aerosol partitioning in and around animal feeding operations in northeastern Colorado in late summer 2021. J. Geophys. Res. 129, e2023JD040507, doi:10.1029/2023JD040507, 2024.

Li, Y., Barth, M. C., Patton, E. G., and Steiner, A. L.: Impact of in-cloud aqueous processes on the chemistry and transport of biogenic volatile organic compounds, J. Geophys. Res., 122, 11,131–11,153, doi:10.1002/2017JD026688, 2017.

https://doi.org/10.5194/egusphere-2025-6552
Preprint. Discussion started: 23 January 2026

McNeill, V. F.: Aqueous organic chemistry in the atmosphere: Sources and chemical processing of organic aerosols, Environ. Sci. & Tech., 49 (3), 1237-1244, doi: 10.1021/es5043707, 2015.

Mitra, S. K., Brinkmann, J., and Pruppacher, H. R.: A wind-tunnel study on the drop-to-particle conversion. J. Aerosol Sci., 23, 245–256, doi:10.1016/0021-8502(92)90326-Q, 1992.

Nault, B. A., Garland, C., Pusede, S. E., Wooldridge, P. J., Ullmann, K., Hall, S. R., and Cohen, R. C.: Measurements of $CH_3O_2NO_2$ in the upper troposphere, Atmos. Meas. Tech., 8, 987–997, doi:10.5194/amt-8-987-2015, 2015.

Nault, B.. A., Garland, C., Wooldridge, P. J., Brune, W. H., Campuzano-Jost, P., Crounse, J. D., Day, D. A., Dibb, J., Hall, S. R., Huey, L. G., Jimenez, J. L., Liu, X., Mao, J., Mikoviny, T., Peischl, J., Pollack, I. B., Ren, X., Ryerson, T. B., Scheuer, E., Ullmann, K., Wennberg, P. O.,Wisthaler, A., Zhang, L., Cohen, R. C.: Observational constraints on the oxidation of NOx in the upper troposphere. J. Phys. Chem. A, 120, 1441-1451, doi: 10.1021/acs.jpca.5b07824, 2016.

Nault, B. A., Campuzano-Jost, P., Day, D. A., Jo, D. S., Schroder, J. C., Allen, H. M., Bahreini, R., Bian, H., Blake, D. R., Chin, M., Clegg, S. L., Colarco, P. R., Crounse, J. D., Cubison, M. J., DeCarlo, P. F., Dibb, J. E., Diskin, G. S., Hodzic, A., Hu, W., Katich, J. M., Kim, M. J., Kodros, J. K., Kupc, A., Lopez-Hilfiker, F. D., Marais, E. A., Middlebrook, A. M., Andrew Neuman, J., Nowak, J. B., Palm, B. B., Paulot, F., Pierce, J. R., Schill, G. P., Scheuer, E., Thornton, J. A., Tsigaridis, K., Wennberg, P. O., Williamson, C. J., and Jimenez, J. L.: Chemical transport models often underestimate inorganic aerosol acidity in remote regions of the atmosphere, Commun. Earth Environ., 2, 1–13, doi:10.1038/s43247-021-00164-0, 2021.

Noone, K.J., Ogren, J.A., Hallberg, A., Heintzenberg, J., Ström, J., Hansson, H.-C., Svenningsson, B., Wiedensohler, A., Fuzzi, S., Facchini, M.C., Arends, B.G. and Berner, A.: Changes in aerosol size- and phase distributions due to physical and chemical processes in fog, Tellus B: Chem. Phys. Meteor., 44(5), p. 489-504. doi:10.3402/tellusb.v44i5.15563, 1992.

NWS Environmental Parameters and Indices, https://www.weather.gov/lmk/indices, last accessed 2025.

Ohata, S., Moteki, N., Mori, T., Koike, M., and Kondo, Y.: A key process controlling the wet removal of aerosols: New observational evidence. Sci. Rep., 6, 34113, doi: 10.1038/srep34113, 2016.

Pye, H. O. T., Nenes, A., Alexander, B., Ault, A. P., Barth, M. C., Clegg, S. L., Collett Jr., J. L., Fahey, K. M., Hennigan, C. J., Herrmann, H., Kanakidou, M., Kelly, J. T., Ku, I.-T., McNeill, V. F., Riemer, N., Schaefer, T., Shi, G., Tilgner, A., Walker, J. T., Wang, T., Weber, R., Xing, J., Zaveri, R. A., and Zuend, A.: The acidity of atmospheric particles and clouds, Atmos. Chem. Phys., 20, 4809–4888, doi:10.5194/acp-20-4809-2020, 2020.

Rolph, G., Stein, A., Stunder, B.: Real-time Environmental Applications and Display sYstem: READY. Environmental Modelling & Software, 95, 210-228, doi:10.1016/j.envsoft.2017.06.025, 2017.

https://doi.org/10.5194/egusphere-2025-6552
Preprint. Discussion started: 23 January 2026

Schill, G. P., Froyd, K. D., Bian, H., Kupc, A., Williamson, C., Brock, C. A., Ray, E., Hornbrook, R.S., Hills, A. J., Apel, E. C., Chin, M., Colarco, P. R., Murphy, D. M.: Widespread biomass burning smoke throughout the remote troposphere. Nature Geoscience 13, 422–427. doi:10.1038/s41561-020-0586-1, 2020.

Schroder, J. C., Campuzano-Jost, P., Day, D. A., Shah, V., Larson, K., Sommers, J. M., Sullivan, A. P., Campos, T., Reeves, J. M., Hills, A., Hornbrook, R. S., Blake, N. J., Scheuuer, E., Guo, H., Fibiger, D. L., McDuffie, E. E., Hayes, P. L., Weber, R. J., Dibb, J. E., Apel, E. C., Jaegle, L., Brown, S. S., Thornton, J. A., Jimenez, J. L.: Sources and secondary production of organic aerosols in the northeastern United States during WINTER. J. Geophys. Res., 123, 7771–7796. doi:10.1029/2018JD028475, 2018.

Schueneman, M. K., Nault, B. A., Campuzano-Jost, P., Jo, D. S., Day, D. A., Schroder, J. C., Palm, B. B., Hodzic, A., Dibb, J. E., and Jimenez, J. L.: Aerosol pH indicator and organosulfate detectability from aerosol mass spectrometry measurements, Atmos. Meas. Tech., 14, 2237–2260, doi:10.5194/amt-14-2237-2021, 2021.

Seinfeld, J. H. and Pandis, S. N.: Atmospheric Chemistry and Physics: From Air Pollution to Climate Change. Third Edition. John Wiley & Sons, Inc, 2016.

Skamarock, W. C., Powers, J. G., Barth, M., Dye, J. E., Matejka, T., Bartels, D., Baumann, K., Stith, J., Parrish, D. D., Hubler, G.: Numerical simulations of the July 10 Stratospheric-Tropospheric Experiment: Radiation, Aerosols, and Ozone/Deep Convection Experiment convective system: Kinematics and transport, J. Geophys. Res., 105, 19,973-19,990, doi:10.1029/2000JD900179, 2000.

Sorooshian, A., Lu, M.-L., Brechtel, F. J., Jonsson, H., Feingold, G., Flagan, R. C., and Seinfeld, J. H.: On the source of organic acid aerosol layers above clouds. Environ. Sci. Tech., 41(13), 4647–4654. doi:10.1021/es0630442, 2007.

Stein, A. F., Draxler, R. R, Rolph, G. D., Stunder, B. J. B., Cohen, M. D., and Ngan, F., (). NOAA's HYSPLIT atmospheric transport and dispersion modeling system, Bull. Amer. Meteor. Soc., 96, 2059-2077, doi:10.1175/BAMS-D-14-00110, 2015.

Takegawa, N., Miyakawa, T., Kawamura, K., and Kondo, Y.: Contribution of selected dicarboxylic and ω-oxocarboxylic acids in ambient aerosol to the m/z 44 signal of an aerodyne aerosol mass spectrometer. Aerosol Sci. Tech., 41(4), 418–437. doi:10.1080/02786820701203215, 2007.

Textor, C., Schulz, M., Guibert, S., Kinne, S., Balkanski, Y., Bauer, S. E., Berntsen, T., Berglen, T. F., Boucher, O., Chin, M., Dentener, F., Diehl, T., Easter, R., Feichter, J., Fillmore, D., Ghan, S., Ginoux, P., Gong, S., Grini, A., Hendricks, J., Horowitz, L., Huang, P., Isaksen, I., Iversen, T., Kloster, S., Koch, D., Kirkevåg, A., Kristjansson, J. E., Krol, M., Lauer, A., Lamarque, J. F., Liu, X., Montanaro, V., Myhre, G., Penner, J., Pitari, G., Reddy, S., Seland, O., Stier, P., Takemura, T., and Tie, X.: Analysis and quantification of the diversities of aerosol life cycles within AeroCom, Atmos. Chem. Phys., 6, 1777–1813, doi: 10.5194/acp-6-1777-2006, 2006.

https://doi.org/10.5194/egusphere-2025-6552
Preprint. Discussion started: 23 January 2026

Toon, O. B., Maring, H., Dibb, J., Ferrare, R., Jacob, D. J., Jensen, E. J., Luo, Z. J., Mace, G. G., Pan, L. L., Pfister, L., Rosenlof, K. H., Redemann, J., Reid, J. S., Singh, H. B., Thompson, A. M., Yokelson, R., Minnis, P., Chen, G., Jucks, K. W., and Pszenny, A.: Planning, implementation, and scientific goals of the Studies of Emissions and Atmospheric Composition, Clouds and Climate Coupling by Regional Surveys (SEAC^{4}RS) field mission, J. Geophys. Res., 121, 4967–5009, doi:10.1002/2015JD024297, 2016.

Tost, H.: Chemistry–climate interactions of aerosol nitrate from lightning, Atmos. Chem. Phys., 17, 1125–1142, doi:10.5194/acp-17-1125-2017, 2017.

Tsui, W. G., Woo, J. L., and McNeill, V. F.: Impact of aerosol-cloud cycling on aqueous secondary organic aerosol formation, Atmosphere, 10, 666–666, doi:10.3390/atmos10110666, 2019.

Yang, Q., Easter, R. C., Campuzano-Jost, P., Jimenez, J. L., Fast, J. D., Ghan, S. J., Wang, H., Berg, L. K., Barth, M. C., Liu, Y., Shrivastava, M. B., Singh, B., Morrison, H., Fan, J., Ziegler, C. L., Bela, M., Apel, E., Diskin, G. S., Mikoviny T., and Wisthaler, A.: Aerosol transport and wet scavenging in deep convective clouds: A case study and model evaluation using a multiple passive tracer analysis approach. J. Geophys. Res., 120, 8448–8468, doi:10.1002/2015JD023647, 2015.

Yatavelli, R. L. N., Mohr, C., Stark, H., Day, D. A., Thompson, S. L., Lopez-Hilfiker, F. D., Campuzano-Jost, P.,. Palm, B. B., Vogel, A. L., Hoffmann, T., Heikkinen, L., Äijälä, M., Ng, N. L., Kimmel, J. R., Canagaratna, M. R., Ehn, M., Junninen, H., Cubison, M. J., Petäjä, T., Kulmala, M., Jayne, J. T., Worsnop, D. R., and Jimenez, J. L.: Estimating the contribution of organic acids to northern hemispheric continental organic aerosol, Geophys. Res. Lett., 42, 6084–6090, doi:10.1002/2015GL064650, 2015.

Yu, J. Z., Huang, X.-F., Xu, J., and Hu, M.: When aerosol sulfate goes up, so does oxalate: Implication for the formation mechanisms of oxalate. Environ. Sci. Tech., 39(1), 128–133. doi:10.1021/es049559f, 2005.

Yu, P., Froyd, K. D., Portmann, R. W., Toon, O. B., Freitas, S. R., Bardeen, C. G., Brock, C., Fan, T., Gao, R., Katich, J. M., Kupc, A., Liu, S., Maloney, C., Murphy, D. M., Rosenlof, K. H., Schill, G., Schwarz, J. P., and Williamson, C.: Efficient in-cloud removal of aerosols by deep convection. Geophys. Res. Lett., 46, 1061–1069. doi:10.1029/2018GL080544, 2019.

Zheng G, Su H, Cheng Y. Role of carbon dioxide, ammonia, and organic acids in buffering atmospheric acidity: The distinct contribution in clouds and aerosols. Environ Sci Technol., 57 (34), 12571-12582. doi: 10.1021/acs.est.2c09851, 2023.

Ziemba, L. D., Griffin, R. J., Whitlow, S., and Talbot, R. W.: Characterization of water-soluble organic aerosol in coastal New England: Implications of variations in size distribution. Atmos. Environ., 45(39), 7319–7329. doi:10.1016/j.atmosenv.2011.08.022, 2011.